ΠΑΝΕΠΙΣΤΗΜΙΟ ΘΕΣΣΑΛΙΑΣ
ΣΧΟΛΗ ΘΕΤΙΚΩΝ ΕΠΙΣΤΗΜΩΝ
ΤΜΗΜΑ ΠΛΗΡΟΦΟΡΙΚΗΣ ΜΕ ΕΦΑΡΜΟΓΕΣ ΣΤΗ ΒΙΟΙΑΤΡΙΚΗ

ΜΟΝΤΕΛΟΠΟΙΗΣΗ ΚΑΙ ΈΛΕΓΧΟΣ ΕΥΚΑΜΠΤΗΣ ΠΤΥΣΣΟΜΕΝΗΣ ΡΟΜΠΟΤΙΚΗΣ ΔΙΑΤΑΞΗΣ ΓΙΑ ΤΗΝ ΈΓΚΑΙΡΗ ΔΙΑΓΝΩΣΗ ΤΟΥ ΚΑΡΚΙΝΟΥ ΤΟΥ ΜΑΣΤΟΥ

ΚΟΥΜΠΟΓΙΑΝΝΗ ΧΡΙΣΤΙΝΑ

ΠΤΥΧΙΑΚΗ ΕΡΓΑΣΙΑ

Επιβλέπων
ΒΑΡΘΟΛΟΜΑΙΟΣ ΠΑΝΑΓΙΩΤΗΣ
Επίκουρος Καθηγητής

Λαμία, 2024

Modeling and Control of an eversion growing Robot for Early Diagnosis in Breast Cancer

Christina Koumpogianni
Senior's thesis

July 12, 2024

Supervisor: Dr. Vartholomeos Panagiotis

University of Thessaly
Department of Computer Science and Biomedical Informatics

Lamia, Greece

Με ατομική μου ευθύνη και γνωρίζοντας τις κυρώσεις (1), που προβλέπονται από της διατάξεις της παρ. 6 του άρθρου 22 του Ν. 1599/1986, δηλώνω ότι:

1. *Δεν παραθέτω κομμάτια βιβλίων ή άρθρων ή εργασιών άλλων αυτολεξεί* ***χωρίς να τα περικλείω σε εισαγωγικά*** *και χωρίς να αναφέρω το συγγραφέα, τη χρονολογία, τη σελίδα. Η αυτολεξεί παράθεση χωρίς εισαγωγικά χωρίς αναφορά στην πηγή, είναι λογοκλοπή. Πέραν της αυτολεξεί παράθεσης, λογοκλοπή θεωρείται και η παράφραση εδαφίων από έργα άλλων, συμπεριλαμβανομένων και έργων συμφοιτητών μου, καθώς και η παράθεση στοιχείων που άλλοι συνέλεξαν ή επεξεργάσθηκαν, χωρίς αναφορά στην πηγή.*
2. *Δέχομαι ότι η αυτολεξεί* ***παράθεση χωρίς εισαγωγικά****, ακόμα κι αν συνοδεύεται από αναφορά στην πηγή σε κάποιο άλλο σημείο του κειμένου ή στο τέλος του, είναι αντιγραφή. Η αναφορά στην πηγή στο τέλος π.χ. μιας παραγράφου ή μιας σελίδας, δεν δικαιολογεί συρραφή εδαφίων έργου άλλου συγγραφέα, έστω και παραφρασμένων, και παρουσίασή τους ως δική μου εργασία.*
3. *Δέχομαι ότι υπάρχει επίσης περιορισμός στο μέγεθος και στη συχνότητα των παραθεμάτων που μπορώ να εντάξω στην εργασία μου εντός εισαγωγικών. Κάθε μεγάλο παράθεμα (π.χ. σε πίνακα ή πλαίσιο, κλπ), προϋποθέτει ειδικές ρυθμίσεις, και όταν δημοσιεύεται προϋποθέτει την άδεια του συγγραφέα ή του εκδότη. Το ίδιο και οι πίνακες και τα σχέδια.*
4. *Δέχομαι όλες τις συνέπειες σε περίπτωση λογοκλοπής ή αντιγραφής.*

Ημερομηνία: 20 Οκτωβρίου 2023

Ο – Η Δηλ.

(Υπογραφή)

(1) «Όποιος εν γνώσει του δηλώνει ψευδή γεγονότα ή αρνείται ή αποκρύπτει τα αληθινά με έγγραφη υπεύθυνη δήλωση του άρθρου 8 παρ. 4 Ν. 1599/1986 τιμωρείται με φυλάκιση τουλάχιστον τριών μηνών. Εάν ο υπαίτιος αυτών των πράξεων σκόπευε να προσπορίσει στον εαυτόν του ή σε άλλον περιουσιακό όφελος βλάπτοντας τρίτον ή σκόπευε να βλάψει άλλον, τιμωρείται με κάθειρξη μέχρι 10 ετών.

Contents

1 Introduction **1**
1.1 Motivation and Significance of this work 1
1.2 Structure of the thesis 2
1.3 Contribution of the thesis 4

2 Literature Review and State of the Art **7**
2.1 Introduction 7
2.2 Classification and Description 8
2.2.1 Archaeological Application 8
2.2.2 Nuclear Application 8
2.2.3 Industrial Application 10
2.2.4 Agricultural Application 10
2.2.5 Medical Applications 11
2.3 Literature review of eversion-growing robotic systems for Minimally Invasive Surgery (MIS) 12
2.4 Modeling of eversion-growing robotic systems 14
2.5 MAMMOBOT system description and architecture 16
2.6 Conclusions 17

3 Modeling of DC motor and rack-pinion dynamics **19**
3.1 Introduction 19
3.2 Mathematical model 22
3.2.1 Power Variables 22
3.2.2 Two-Port Energy Transducing Elements - Transformers 24
3.2.3 Linear Graph, Normal Tree and Links formulation 25
3.2.4 Variables of the system 28
3.2.5 Elemental equations of of DC motor and rack-pinion dynamics 30
3.2.6 Continuity equations of of DC motor and rack-pinion dynamics 31
3.2.7 Compatibility equations of of DC motor and rack-pinion dynamics 33
3.2.8 Final elemental equations after substitution 34
3.2.9 State equations of DC motor and rack-pinion dynamics 36
3.2.10 Matrix formulation 38
3.3 Simulation results 40
3.4 Conclusions 43

4 Modeling of eversion system and of complete system **45**

4.1 Introduction 45
4.2 Mathematical model 46
4.2.1 Two-Port Energy Transducing Elements - Gyrators 46
4.2.2 Linear Graph, Normal Tree and Links formulation 47
4.2.3 Variables of the system 49
4.2.4 Elemental equations of the complete system 52
4.2.5 Continuity equations of the complete system 53
4.2.6 Compatibility equations of the complete system 53
4.2.7 Final elemental equations after substitution 54
4.2.8 State equations of the complete system 55
4.2.9 Matrix Formulation 57
4.3 Forces and Frictions 58
4.4 Simulation results 60
4.5 Conclusions 66

5 Automatic Control System 67

6 Control of the complete system 69

7 Conclusions 77

Bibliography 79

Chapter 1

Introduction

1.1 Motivation and Significance of this work

The motivation behind this thesis is the potential for earlier cancer detection and improved outcomes facilitated by the utilization of the eversion growing robot model, offering improved intervention and treatment. Early detection of breast cancer increases significantly survival rate and reduces the economic burden on the healthcare system. The International Agency for Research on Cancer (IARC) have released the amount of people that suffered due to cancer: in 2022, there was an estimated 20 million new cancer cases and 9.7 million deaths. World health organization also published survey results from 115 countries, showing that a number of countries do not adequately finance priority cancer and palliative care services, as part of universal health coverage utilizing advanced micro-endoscopy methods could lead to substantial rise in early diagnosis.

The three major types of cancer in 2022 were lung, breast and colorectal cancer. Lung cancer was the most commonly occurring cancer worldwide with 2.5 million new cases accounting for 12.4% of the total new cases. Female breast cancer ranked second (2.3 million cases, 11.6%), followed by colorectal cancer (1.9 million cases, 9.6%). [12]. The technical challenges that still exist, along with the extremely small anatomical dimensions have not allowed yet the advancement of endoscopic diagnosis in breast cancer detection.

In 2022, breast cancer resulted in 670.000 fatalities worldwide. Around half of all breast cancer cases manifest in women without identifiable risk factors apart from their gender and age. Breast cancer stood out as the primary cancer affecting women in 157 out of 185 countries in 2022, showcasing its global prevalence. It is noteworthy that breast cancer occurs in every nation across the globe, highlighting its widespread impact. Additionally, while comparatively rare, approximately 0.5-1 % of breast cancer incidents are observed in men [11]. Detection will reduce the economic burden of treatment, as surgical intervention and chemoradiotherapy will be avoided. eversion growing robots, could be an excellent solution to this problem, as they could provide endoscopic tools that can adjust to their environment, minimizing the impact on the tissues and blood vessels. Moreover, the everting technique could eliminate frictions with the tissue walls, enabling safe navigation through the vessels without causing trauma or any other problems to the patient. Additionally, one more advantage of using this everting technique is that these robots can be adjusted to each patient's anatomical structural characteristics due to their compliance, making them personalized and suitable for individual needs. Until now, the most common detection methods that are used for breast cancer are mammograms (X-ray picture of the breast), ultrasound, and breast MRI (Magnetic Resonance Imaging). Other tests, such as CT scans, bone scans, or PET scans might sometimes be done to help find out if breast cancer has spread. Newer types of tests are now being developed for breast imaging. Some of these, such as breast tomosynthesis (3D mammography), are already being used in some centers [18]. The case in point is robot Mammobot, because it is related to breast cancer diagnosis and because we can have access to data due to our collaboration with King's College London team, in the context of EU project Softreach [19].

1.2 Structure of the thesis

The model that is represented in this thesis is a soft growing robotic system which consists of the following parts: a Direct Current (DC) motor, a rack and pinion system and a pneumatic system that is a tube which inside contains the growing element. The DC motor combines the elecromagnetic subsystem with the mechanical one, providing energy to the entire system to achieve rotational and, subsequently, linear velocity to the rack. The pinion is attached to the rack in order to transform the rotational motion into linear. The rack and pinion mechanical system represent the active channel that controls the velocity and the behaviour of the growing element. The growing element is inside a tube compressed with gas, and represents the pneumatic subsystem.

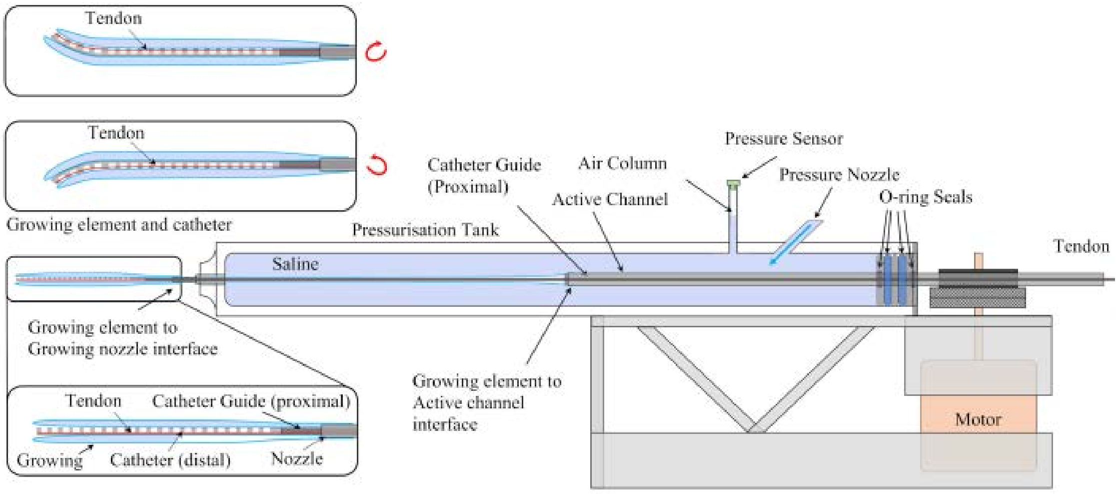

Figure 1.1: Illustration of Mammobot's elements: DC motor, Active channel and Growing element. Cross section of the pressurisation tank showing the interface between the growing element and both the active channel and the growing nozzle [3].

The system's architecture that is going to be analyzed in the thesis based on figure 1.1 lies in the dashed line delimited box:1.2.

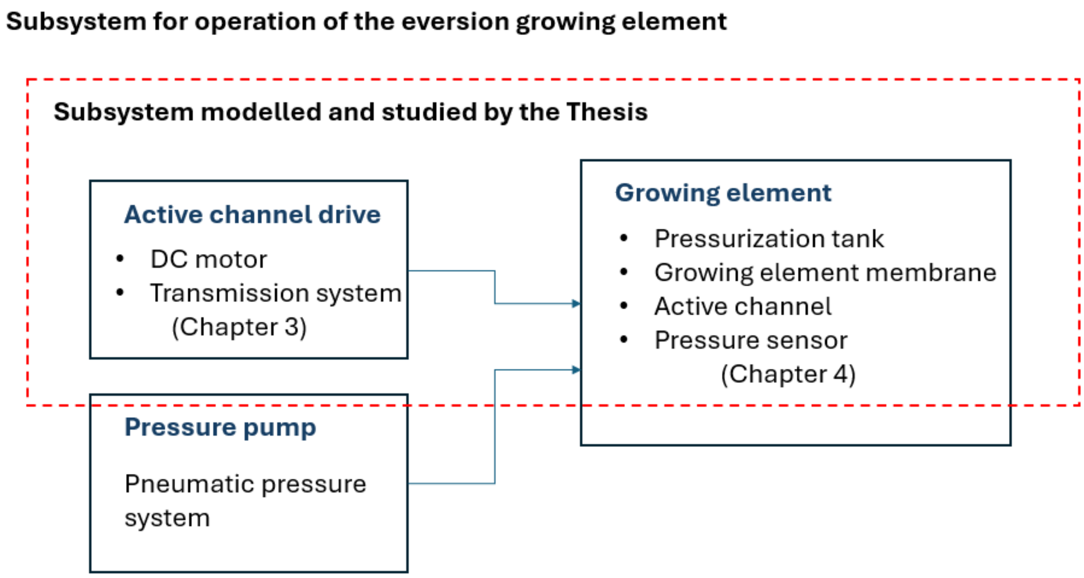

Figure 1.2: Structure of the system.

For a more comprehensive and detailed analysis, this thesis is structured into two specific sections. The first section focuses on the DC motor, which is integral to the system, examining its interaction with the rack and pinion mechanism. Then, it delves into the motor's operational principles, its role in converting electrical energy

into mechanical energy, and how it provides the rotational and linear motion necessary for the system's functionality.
The second section examines the eversion subsystem, a significant component that influences the overall behavior and performance of this mechatronic system. The design, operation, and impact of the eversion system on the system's efficiency and effectiveness is examined too. The comprehensive analysis aims to provide a thorough understanding of how each component interacts within the system. Generally, all the mechanisms involved are going to be studied and analyzed in depth. The developed comprehensive physical and mathematical models, as well as the differential equations will provide the necessary knowledge for the system's operation and effectiveness.
In the third section, a nonlinear model based controller was developed to guarantee the robot's control performance. A closed loop control will be implemented using proportional control, in order to control the growing element's velocity according to the user's needs.
This thesis focuses on the detailed analysis of each subsystem that described above by formulating in a systematic way state equations that govern each system. These collectively form the mathematical model. Following the development of this model, simulation results are presented and analyzed, leading to the conclusions that will be discussed comprehensively.
All these together will provide the necessary results to evaluate if this growing robot is effective for its aim, easy to operate and implement in everyday life. The conclusions at the end of each part will finally summarize all these findings and come into a conclusion if this robot can come up with the expectations outlined in the section of motivation and the significance.

1.3 Contribution of the thesis

The contribution of this thesis lies in the thorough analysis of a dynamic model formulation of the mechatronic system of an eversion growing element endoscope. The computational complexity of the dynamic model allows for real-time control and will contribute to achieve a new, non-complex way of breast cancer detection that is more effective, painless and will decrease significantly the death rate due to early detection in the first stages of cancer obtruding its spreading. The real-time control will enable the lead doctor to navigate through the blood vessels, providing full visibility of the interior and without causing any damage. The operator will input each time the necessary parameters required for the system's desired velocity and behavior, ensuring it functions according to the needs and the structure of each breast cancer case. A closed loop control study for the automatic control of the growing element speed achieved this function. Adjustments to the system's input sources will provide the desired velocity and motion of the growing element.

Chapter 2

Literature Review and State of the Art

2.1 Introduction

Eversion-vine (Vascular Internal Navigation by Extension) robotic systems, also called eversion growing robots, represent a significant innovation in the robotics industry. Due to their unique construction, which consists of a soft membrane that can be everted multiple times its original length through their tip, their movement relies on growth instead of simply walking. They imitate the motion of vine plants; specifically, they have a grounded base (root) and can continually grow by adding material-membrane at their tip as they expand [22]. The first theoretical and practical approach was implemented in 2017 by the Stanford's University research team, led by Professor Allison Okamura, with the key individual credited with the initial idea and development being Elliot Hawkes, who was a PhD student in Prof. Okamura's lab at the time. The basic principles behind this implementation were the usage of pressurization of an inverted thin-walled vessel in order to achieve rapid and substantial lengthening of the tip of the robot body, and the control of the asymmetric lengthening of the tip that offers directional control [7]. Due to their unique and soft construction, they are ideal for search and rescue purposes, such as searching for human lives in ruins, exploring collapsed structures, confined spaces and even sending food to trapped people. They are also suitable for deployable structures like helical antennas [22]. This innovative robotic system has triggered ongoing research to explore its implementation in various fields. Their classification spans several branches, including archaeology, nuclear facilities, industry, agriculture and the latest one is medicine, for minimal invasive surgery.

2.2 Classification and Description

2.2.1 Archaeological Application

The basic characteristics of these continuum everting robotic systems are the tip extension,the significant change of length (almost a hundred times its initial length), and directional precise real-time control [4]. In the archaeological field, searches have proved that they can navigate in the environment with precise guidance and move over rocks through horizontal and vertical turns. This was the first usage of vine robot, and was implemented by Stanford's team [4]. The vine robotic tip can successfully move through any obstacle without causing damage, proving that this new method of robotic system can be very helpful, precise and efficient. The following picture 2.1 demonstrates a representation of the vine robot's movement underground in different angles (horizontally and vertically) and proves the ability of navigating through tiny tunnels and of teleoperation.

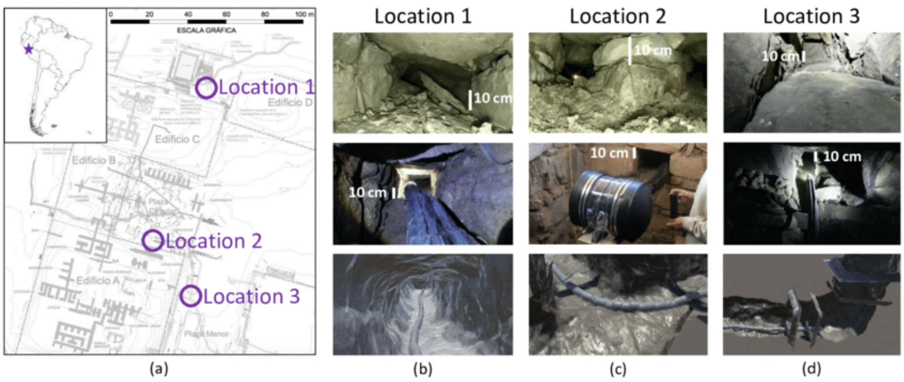

Figure 2.1: Map, photos, and simulation of the vine robot's successful exploration of underground tunnels in an archaeological site in Chavin, Peru. (a) A map of the archaeological site. Areas the vine robot explored are marked in purple. (b) Location 1: A tunnel almost completely blocked by rocks. (c) Location 2: A tunnel with a 90 degree right hand turn. (d) Location 3: A tunnel that started sloping upwards and then turned completely vertical. Top row are photos from inside the tunnels, middle row are photos of the vine robot in the tunnels, and bottom row are screenshots of the simulation of the vine robot in each tunnel [4].

2.2.2 Nuclear Application

Soft growing vine robots show great potential for navigation and decontamination tasks in the nuclear industry. That's because they can navigate in the environment precisely, reaching effectively areas that are hard to access using traditional rigid bodied robots, they don't lose connection with the handler and the most important benefit is their unique construction: their soft membrane that can take up a hundred times its original size and can adopt to the environmental changes, adjusting their diameter constantly. The robot is operated via a control panel, making it easy for humans to control using buttons linked to an Arduino. These control signals are then transmitted down a tether to the robot's tip, where they control its axial movement. Additionally, the Arduino is linked to an SMC (Sintered Metal Corporation) pneumatic regulator, which is further connected to a compressor providing pressure to the robot, enabling it to achieve the eversion. This setup enables the operator to manage movement in both parts of the hybrid robot seamlessly from one control panel. There were conducted three experiments that included extinguishing fires 2.2, precision spraying 2.3, and immobilizing objects in order to check the robot's abilities. All these successful experiments highlighted its potential for use in hazardous environments such as nuclear facilities [1].

Figure 2.2: a) Hybrid robot demonstrating its versatility in simulating effectively extinguishing a candle's fire by employing a water-spraying mechanism. b) A POV view of the target, using the built in tip mounted micro camera [1].

Figure 2.3: Hybrid robot showcasing adaptability in simulating Scenario 3, employing an expanding foam application to effectively cover the walls of the glove box. [1]

2.2.3 Industrial Application

In addition, they can be used for industrial inspection, maintenance and repairing because these vine eversion robots can access areas that cannot easily be reached by human or other robots, such as the inside of pipelines, ducts, or machinery. For instance, pipelines are a fundamental component of terrestrial infrastructures and their correct operations are vital to the stability of our societies, considering freshwater supply and sewage. Regular inspection of pipelines can therefore prevent failure events that may lead to a critical disruption of the infrastructure. Robotic systems are a preferable solution over human maintenance, for cost and safety reasons, since it is not required to shut down and empty the pipe [9], preventing temporary problems and deceleration. In the figure below 2.4 is illustrated an example of the application of soft robots inside the pipelines, the ability to navigate through them, as well as the ability to turn vertically or horizontally according to handler's instructions.

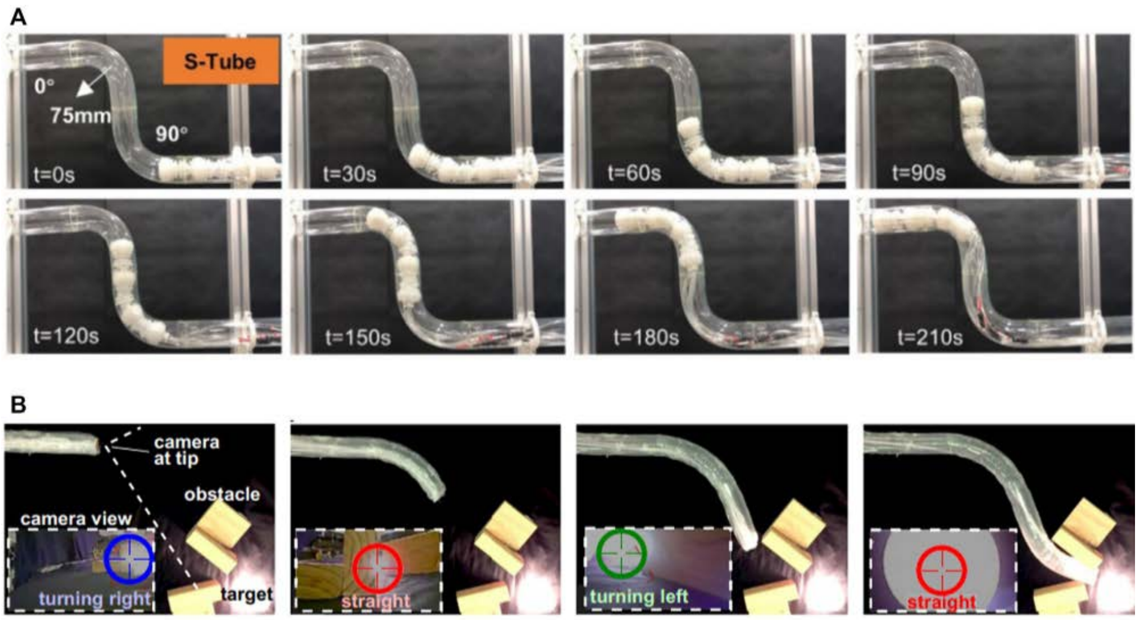

Figure 2.4: Examples of soft robotic systems performing tasks useful for infrastructure protection. (A) Soft crawler navigating an S-shaped pipe (B) Inspection skills of a vine robot [Figure adapted from Hawkes et al. (2017)] [9].

2.2.4 Agricultural Application

Soft robots have a range of various applications, including agriculture. They can be used for harvesting, inspection, monitoring, and weed control. In the tip place of vine robots, apart from cameras, sensors can be incorporated to check environment conditions, and mechanical parts to allow the robot to interact with plants. Due to their ability to grow and move through tight spaces, they can access and pick fruits and vegetables without damaging the plants or produce, unlike other robotic systems that damage the plants. Also, their ability to navigate in the environment without encountering problems from possible obstacles allows them to move through crops to identify and remove weeds without harming the crops. Vine robots can also carry sensors to monitor plant health, soil conditions, and other environmental factors, providing valuable real-time data to farmers. In many of these cases the soft robotic technologies remain in the lab testing phase although their development may be motivated by potential agricultural applications. Further work is required to adapt and optimize the technologies for sustained agricultural deployment [2]. In the following figure 2.5 is represented a break down of agricultural process from seed to fork using soft robotic technologies.

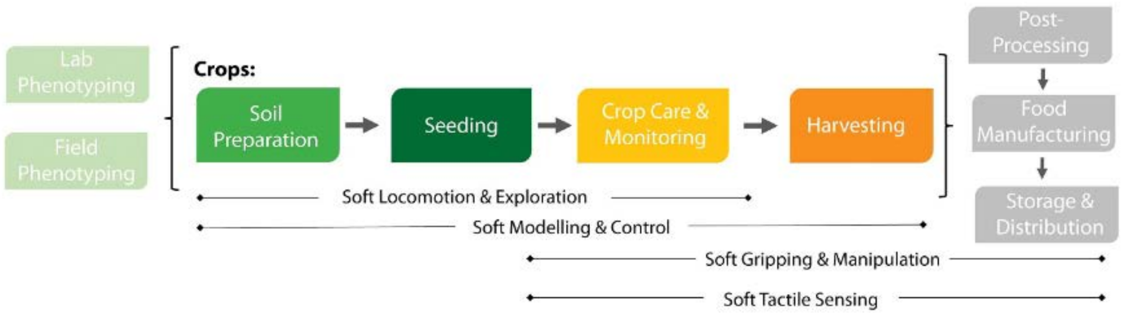

Figure 2.5: Summary of the key processes in arable farming, and the role of soft robotic technologies to be deployed along this process timeline for the various processes [2].

2.2.5 Medical Applications

Vine eversion robots have not started being used in the medical field for minimal invasive surgery yet, but the studies are optimistic that this will be achieved in the coming years due to their rapid development. The application of vine robots in the medical field lies in vine catheters. Vine catheters can be used for endovascular surgery. Pressurized fluid (water or saline) pumped into the base of the VINE catheter enables extension, or lengthening, at the tip, while the rest of the body remains stationary with respect to the environment. The result is a fundamentally different method of movement through the vasculature, which, until this point, has relied on manual and robotic instruments that must be pushed from the base [8]. The catheter will be within the hollow core of the soft membrane, so it will be able to navigate through vessels without causing injuries. As the VINE catheter traverses through the vasculature, it acts as a delivery vehicle by pulling this catheter (termed "inner catheter" here) along. This approach ensures that there is a hollow access channel to the target and sufficient stiffness for treatment to be delivered [8]. This system's function is based on the simple vine robotic's one that mentioned before. In the following figure 2.6 is represented the whole system of the catheter that is inside the vine eversion robot that is controlled with a closed loop system.

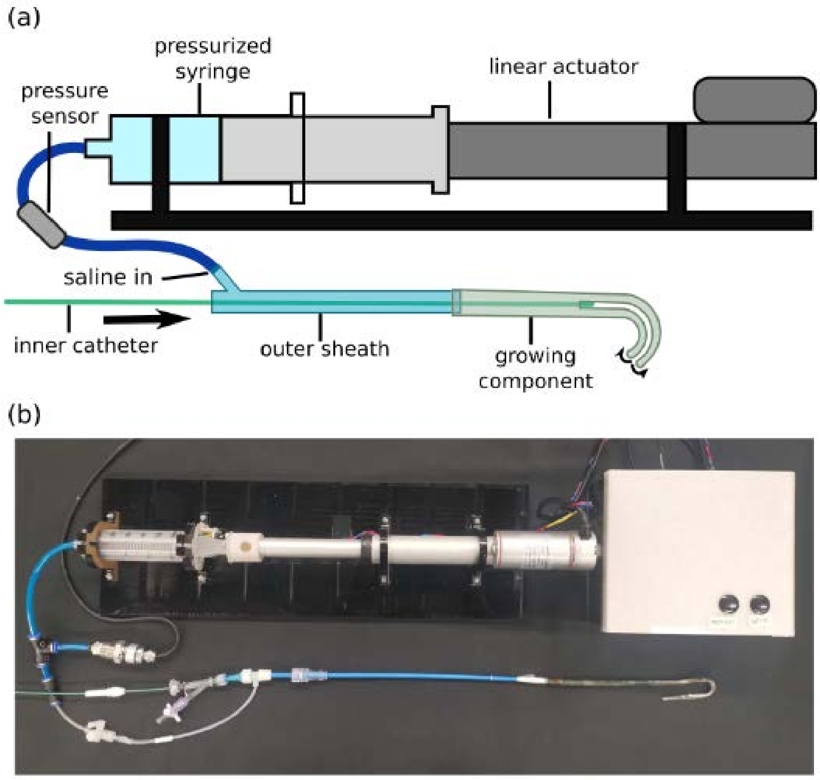

Figure 2.6: (a) Schematic of the entire system, including the actuation system that controls the pressurization of the VINE catheter. (b) Image of the actuation system and closed-loop control box containing the microcontroller and electronics for driving the system. [8].

2.3 Literature review of eversion-growing robotic systems for Minimally Invasive Surgery (MIS)

In order to achieve the implementation of eversion-growing robotic systems in the field of Minimally Invasive Surgery (MIS), certain protection and efficiency measures must be taken into account. Because of their potential usage in human surgery, these robotic systems must be extremely precise, able to navigate safely to avoid injuring tissues, maintain constant connection with the handler, and be made of the softest materials. At the same time, these robots often need a working channel-a hollow core for passing tools (catheters), sensors, and fluids, all of which should be protected from external factors. This makes the hardness of the outside membrane particularly challenging. Recent advancements in bionics, flexible actuation, sensing, and intelligent control algorithms, as well as tunable stiffness, have been referenced when developing soft and flexible robots. By demonstrating the potential capabilities of the flexibility of soft medical robots made of specific bionic materials and structures, their medical application becomes a realistic possibility. Flexible actuation provides power, intelligent control algorithms ensure precise execution, and the wide range of stiffness in the soft materials are three important influencing factors for soft medical robots [23]. However, one challenge to overcome is the increased pressure from internal friction, making it difficult to create miniaturized vine robots (less than 1 cm in diameter) with these channels inside. This is why storing scrunched material at the tip has been developed to reduce this friction. This model has been validated with prototypes as small as 2.3 mm in diameter, enhancing the practicality of miniaturized vine robots for applications like minimally invasive surgery [6]. In Figure 2.7 is illustrated an example of this method that this team has developed as a solution to the problem that mentioned before.

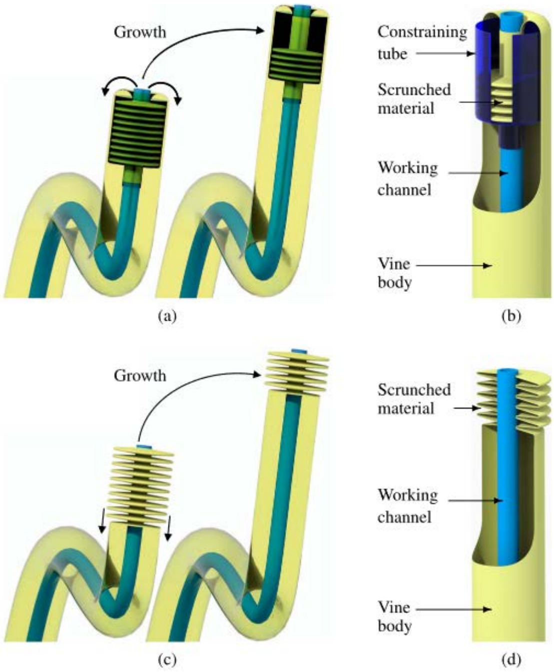

Figure 2.7: Illustration of two new vine robot designs that overcome scaling limitations of current designs with working channels via our proposed concept of material scrunching. (a) The proposed everting scrunched design is shown at two different steps during deployment, along with (b) a zoomed-in view of the tip. (c) The proposed non-everting scrunched design is shown at two steps during deployment, along with (d) a zoomed-in view of the tip [6]

2.4 Modeling of eversion-growing robotic systems

The eversion process involves deploying an inflatable device with a material located at the tip of the robot, which, when under pressure, elongates the robot's body. However, the simulation of this complex kinematic phenomenon is a significant challenge. Dynamic modeling has not been developed yet, but there is an approach of using a combination of kinematics and quasistatic modeling to parameterize the starting conditions of the eversion process. The kinematic model uses the Cosserat rod models for local coordinates, while the quasistatic model is based on finite element analysis. The two models are combined to capture the behavior of the robot tip during eversion. This approach has been implemented and tested using the SOFA framework and has been evaluated on the deployment of a vine robot on a narrow passage [5]. The the part that is pressurized at its tip and is going to be everted is illustrated perfectly in the figure 2.8.The SOFA software was used to model a steerable growing robot, with the robot body represented by a 2D planar thin-walled conical mesh.The finite element method (FEM) is a numerical technique used to solve partial derivative problems. There are no previous literature reviews that have modeled in this way the everting technique, since this team [5]. These results represent only a first step of the modeling of the complete everting technique.

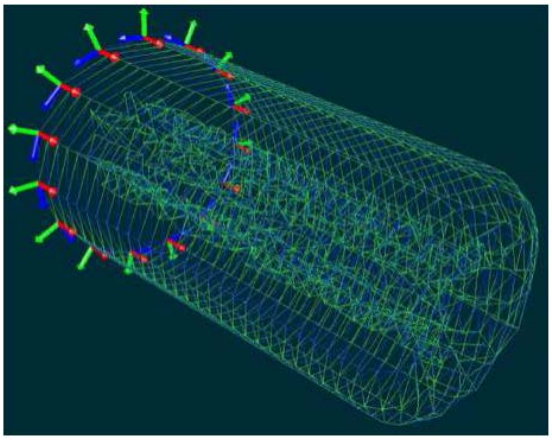

Figure 2.8: Modeling of the eversion of a growing robot by combining the Cosserat rod model with finite element method (FEM) simulation using the SOFA framework [5].

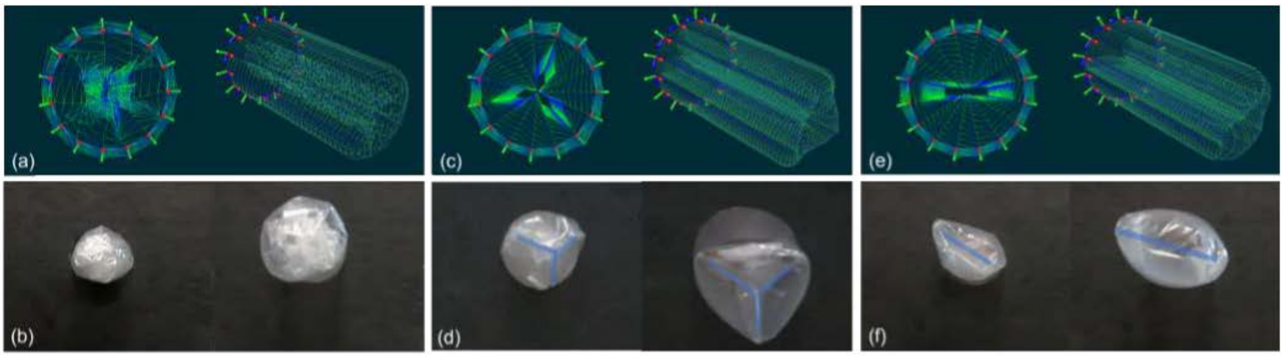

Figure 2.9: Comparison between the simulated (a) (c) (e) and real geometries (b) (d) (f) of the growing robot in the free and imposed cases. The simulated free geometry is represented by a randomly shaped membrane (a), while the simulated imposed geometry is represented by a triangular (c) and linear shape (e) [5].

2.5 MAMMOBOT system description and architecture

MAMMOBOT, is one of the first millimetre-scale steerable soft growing robots for medical applications. It is a specialized type of robotic device designed for medical applications, particularly in the diagnosis and treatment of breast conditions. These robots are typically used in procedures such as breast biopsies, where precise and minimally invasive techniques are crucial. Mammobots use imaging technologies such as MRI or ultrasound, in order to be guided inside tissues. They are extremely tiny and they can navigate in the environment without causing any damage in the tissues like other techniques for breast cancer detection. Mammobot is basically a minature of soft growing eversion robot that inside it a catheter is placed. As shown in the figure 1.1 the Mammobot's elements are: DC motor, active channel, growing element, pressurization tank, pressure nozzle and o-rings seals. The DC motor provides the system with constant power, the active channel is the guide for the growing element, because it is attached to it and according to the velocity of the active channel, the growing element develops the same one. The growing element is the membrane that everts and navigates in the environment, while the pressurization tank due to the high pressure it has, pushes the growing element to evert. The pressure nozzle provides to the tank fluid/air, and the o-rings are attached to the active channel, so by their rotational motion they move the active channel [3].

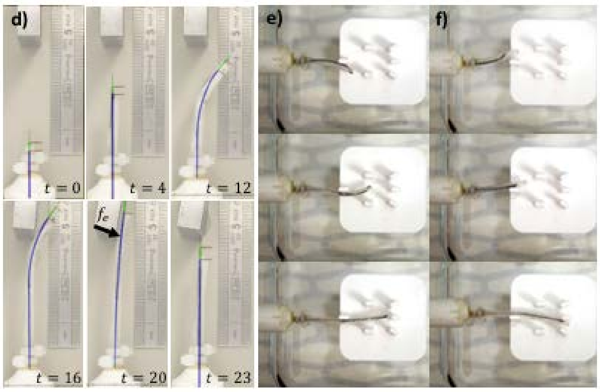

Figure 2.10: (d) The catheter tip position plot is enlarged for better visibility of the simulation and experimental result differences. (e-f) Time lapse of Mammobot navigation. The robot is able to navigate through curved pathways and to avoid obstacles [3].

2.6 Conclusions

This chapter provides an extensive overview of the historical evolution of vine eversion robots, tracing and analyzing their development from 2017, when the Stanford's team developed it, to the present. The chapter highlights the rapid yet stable growth of this new robotic system technique, the everting technique. Based on multiple research studies, this thesis aims to develop dynamic modeling of these robotic systems to achieve a comprehensive understanding of their behavior. Specifically, this thesis is about modelling an eversion growing robot for breast cancer detection, simulating its behavior and providing a nonlinear model with proportional control to guarantee the robot's control performance.

Chapter 3

Modeling of DC motor and rack-pinion dynamics

3.1 Introduction

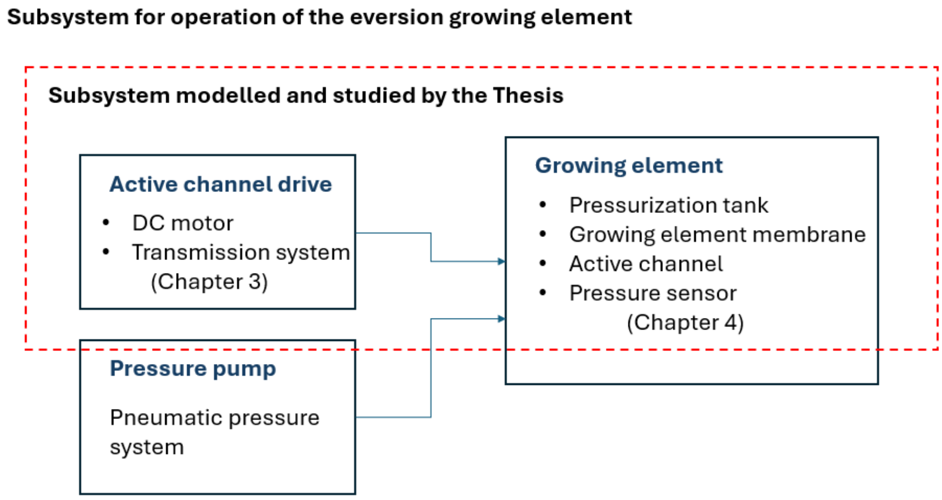

Figure 3.1: Structure of the system.

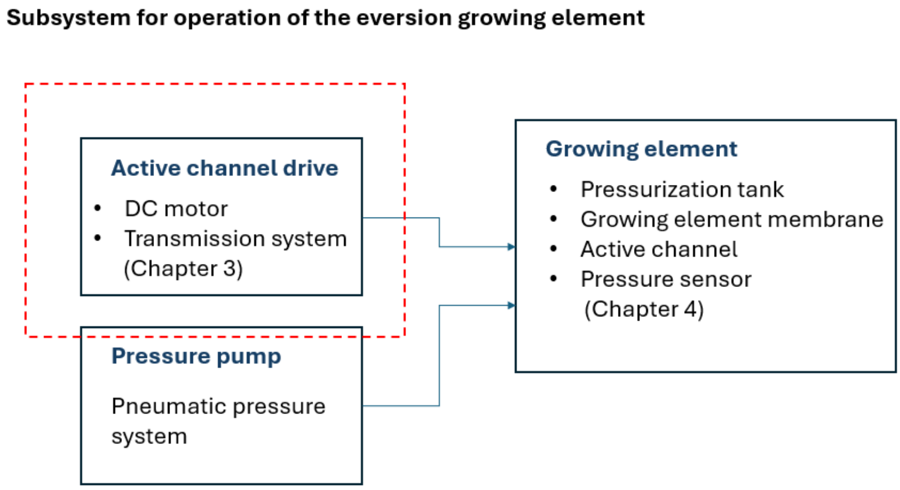

Figure 3.2: System's architecture that is going to be studied in this chapter.

The electrical subsystem 3.3 of the dc motor consists of an inductor L, and a resistor R connected as shown and driven by a voltage source Vs(t). The electromagnetic power that is produced in this part is converted into mechanical one. The mechanic subsystem of the DC motor consists of two rotating gears and it can indeed be described in terms of inertia and friction. The inertia J_1 is a property of an object that quantifies its resistance to changes in its velocity. For a rotating object, the moment of inertia is a measure of how much torque is required for a given angular acceleration and the coefficient of viscous friction B_1 represents the damping force that opposes the rotation, proportional to the angular velocity.

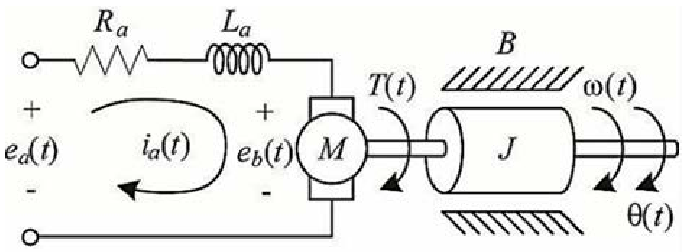

Figure 3.3: Schematic equivalent of DC Motor [15].

The terms that describe the pinion 3.4 are the Inertia J_2 and the coefficient of viscous friction B_2 and the elements that describe the linear motion of the rack are the mass m and the coefficient of depreciation B. In the next chapter the rack will be attached to the active channel and are going to considered as one mass, along with the growing element.

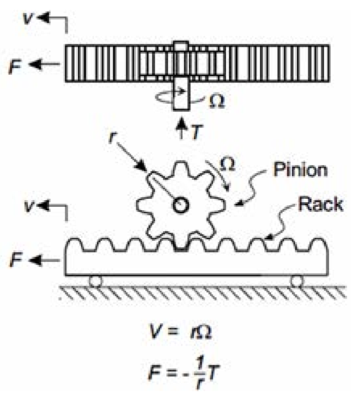

Figure 3.4: Schematic equivalent of rack and pinion dynamics [16].

The type of DC motor that is investigated in this thesis is common in the robotics market. Typical examples of dc motors with permanent magnets can be found in

Maxon company [10]. An example of brushed permanent magnets dc motor is shown in the following pictures:

Figure 3.5: DC Motor [10].

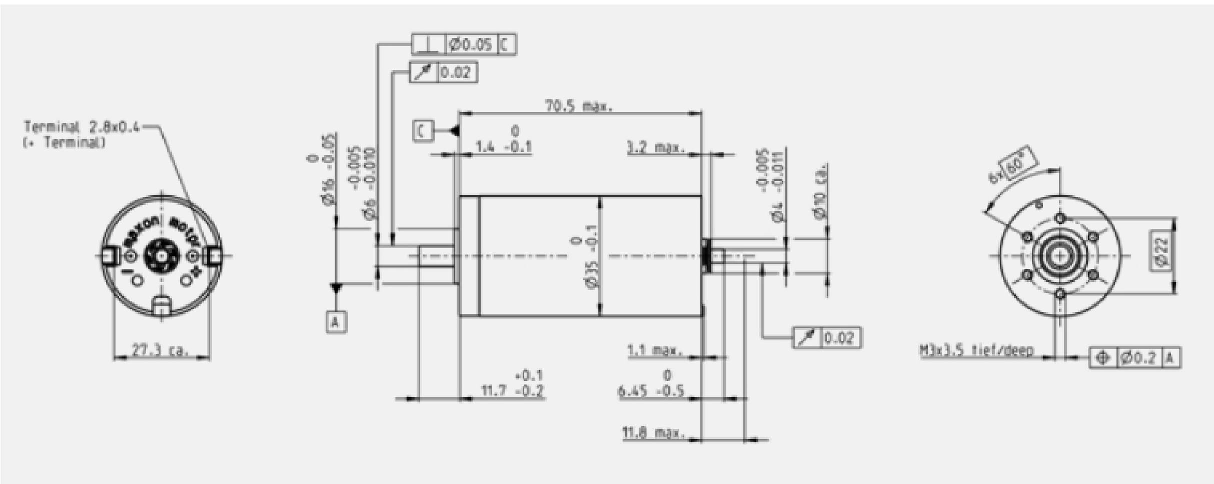

Figure 3.6: Technical illustrations of the DC motor [10].

Based on this specific motor type and its characteristics, a MATLAB code was implemented that describes the behavior of the linear system as a function of time. The values of the parameters that are used in the program that is going to be explained later, are defined by the maxon's motor DCX 35 L, which is a powerhouse with graphite brushes and preloaded ball bearings.

VALUES AT NOMINAL VOLTAGE	
Nominal voltage	12 V
No load speed	8130 rpm
No load current	320 mA
Nominal speed	7610 rpm
Nominal torque (max. continuous torque)	77.7 mNm
Nominal current (max. continuous current)	6 A
Stall torque	2080 mNm
Stall current	152 A
Max. efficiency	86 %

CHARACTERISTICS	
Terminal resistance	0.0788 Ohm
Terminal inductance	0.0263 mH
Torque constant	13.7 mNm/A
Speed constant	699 rpm/V
Speed / torque gradient	4.04 rpm/mNm
Mechanical time constant	4.21 ms
Rotor inertia	99.5 gcm^2

3.2 Mathematical model

3.2.1 Power Variables

In terms of dynamic modeling, all the system's variables are expressed as power variables. It is an approach in systems dynamics that utilizes physical laws, particularly the conservation of energy, to describe the behavior of dynamic systems. By this way, it is more efficient to analyze systems across various domains, such as mechanical, electrical, thermal, and fluid/pneumatic systems. Power variables are quantities whose product gives the rate of energy transfer (power) in a system. They are divided into energy storage elements, energy consumption elements and ideal source elements. The trough variables with the across ones come in pairs. The product of an Through "T" variable and an Across "A" variable gives the power, which is the rate of energy transfer. If the product of the power variables "A" and "T" is positive, then it is assumed that energy is entering the system (the power is positive); otherwise, if it is negative, the system's power flows from the system to the environment (the power is negative).

- If $"T" \cdot "A" > 0,\ P > 0$
- If $"T" \cdot "A" < 0,\ P < 0$

Below lies an example of energy storage fundamental elements in each domain, that can also be referred as through variables "T" [15]:

- Mechanical: Force, torque
- Electrical: Current
- Hydraulic: Flow rate
- Thermal: Temperature difference

Elements that store energy, also referred as Across variables "A":

- Mechanical: Velocity, angular velocity
- Electrical: Voltage
- Hydraulic: Pressure
- Thermal: Heat flow rate

Dissipative elements are the ones that consume energy, also referred as "D" elements: damper, frictions, resistance. Mathematical formulation of power equations in different energy domains:

- Formula for Mechanical Power in Translational Motion:

$$P = F \cdot U \tag{3.1}$$

  where :

  - P = Mechanical Power
  - F = Force: Through Variable "T" [N]
  - U = Linear Velocity: Across Variable "A" [m/s]

- Formula for Mechanical Power in Rotational Motion:

$$P = T \cdot \Omega \tag{3.2}$$

  where :

- P = Mechanical Power
- T = Torque: Through Variable "T" [Nm]
- Ω = Rotational Velocity: Across Variable "A" [rad/s]

- Formula for Hydraulic Power:

$$P = P \cdot Q \tag{3.3}$$

where :

- P = Hydraulic Power
- P = Pressure Drop: Across Variable "A" [N/m^2,Pa]
- Q = Supply, Volume flow: Through Variable "T" [m^3/s]

- For thermodynamic systems, the derivative of power variables does not give power. Power is the variable of the heat flow: P = q [W,J/s], that is a through element "T".

$$q = \frac{dH}{dt} \tag{3.4}$$

where H = Heat [J].

3.2.2 Two-Port Energy Transducing Elements - Transformers

One-port model elements are used to represent energy storage, dissipation, and sources within a single energy domain. In many engineering systems energy is transferred from one energy medium to another; for example in an electric motor electrical energy is converted to mechanical rotational energy, while in a pump mechanical energy is converted into fluid energy. The process of energy conversion between domains is known as transduction and the elements that convert the energy are transducers. Within a single energy domain power may be transmitted from one part of a system to another; for example a speed reduction gear in a rotational system. In this particular system the dc motor converts electrical energy to mechanical one (because of rotational motion) and in rack-pinion subsystem the mechanical energy (due to rotational motion) is converted to mechanical energy (due to translation motion) of the rack. The basic energy transduction processes occurring in these types of devices can be represented by a two-port element, as shown in figure 3.7 in which energy is transferred from one port to another. Each port has a through and an across-variable defined in its own energy domain [17]. Transducers are energy bivalves because they exchange energy from two "ports". Each port corresponds to an energy area with which it communicates.They have four terminals and are described by four power variables, or two pairs of power variables [15].

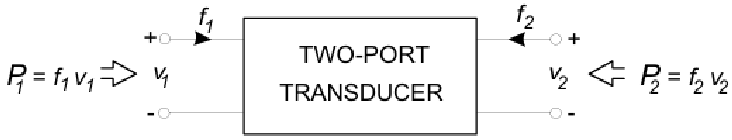

Figure 3.7: Two-port element representation of an energy transducer [17].

Transducers are classified as transformers and gyrators (gyrators will be explain in the next chapter 4).

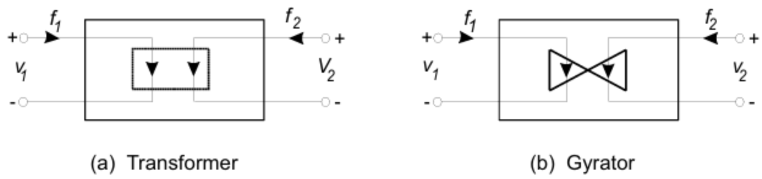

Figure 3.8: Symbolic representation of transforming and gyrating transducers [17].

Transformers are described by the following algebraic expressions:

$$u_2 = TF \cdot u_1 \tag{3.5}$$

$$f_2 = -\frac{1}{TF} \cdot f_1 \tag{3.6}$$

where u_i (i = 1,2) are variables of type "A", f_i (i = 1,2) are variables of type "T" and TF the transformation parameter. Therefore, a transformer algebraically connects variable type "A" with variable of the same type and variable "T" with variable of the same type [15]. If one variable "A" is determined by the system, then the other due to the transformer equation is determined by the (transformer) element. Therefore, only one can be a primary variable. That's why in normal tree representation only one branch can be a primary variable and be included, the other one has to be only secondary and be included as part of the links. In matrix form, the equations governing a transformer are written as follows:

$$\begin{bmatrix} u_2(t) \\ f_2(t) \end{bmatrix} = \begin{bmatrix} TF & 0 \\ 0 & -\frac{1}{TF} \end{bmatrix} \cdot \begin{bmatrix} u_1(t) \\ f_1(t) \end{bmatrix} \tag{3.7}$$

3.2.3 Linear Graph, Normal Tree and Links formulation

Linear graphs represent the physical structure of the system. They are a deconstructed representation of the system's operational principles. Graphs are used for elemental, continuity, compatibility and state equations formulation and have oriented linear branches [15].

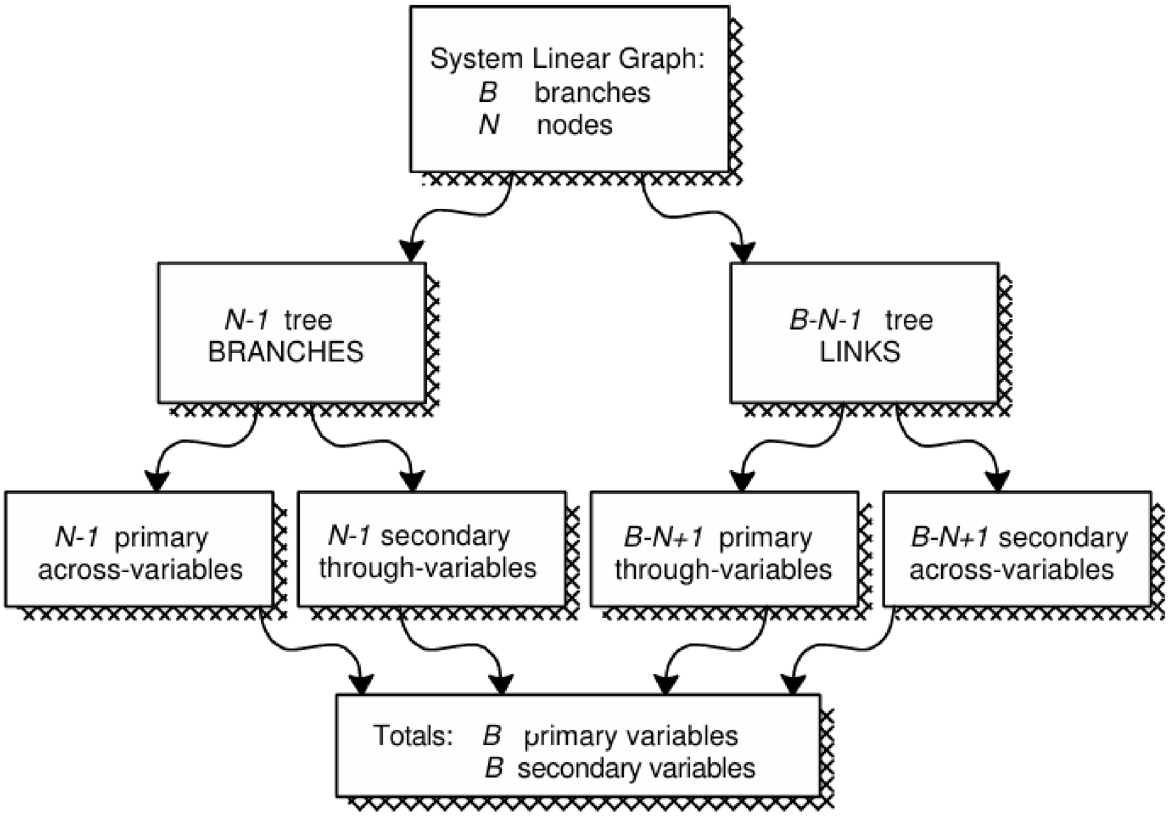

Figure 3.9: System graph variables [16].

A linear graph with B branches represents B system elements, each with a known elemental equation or source function. The graph also represents the structure of the element interconnections, in terms of the continuity and compatibility constraint equations [16]. The nodes represent the across variables "A", that are independent energy storage elements, while the links represent the passive elements "T" that consume energy. Independent energy storage elements are those elements in which the amount of stored energy can be independently determined and controlled. The variables of this graph are explained analytically in chapter 3.2.4.

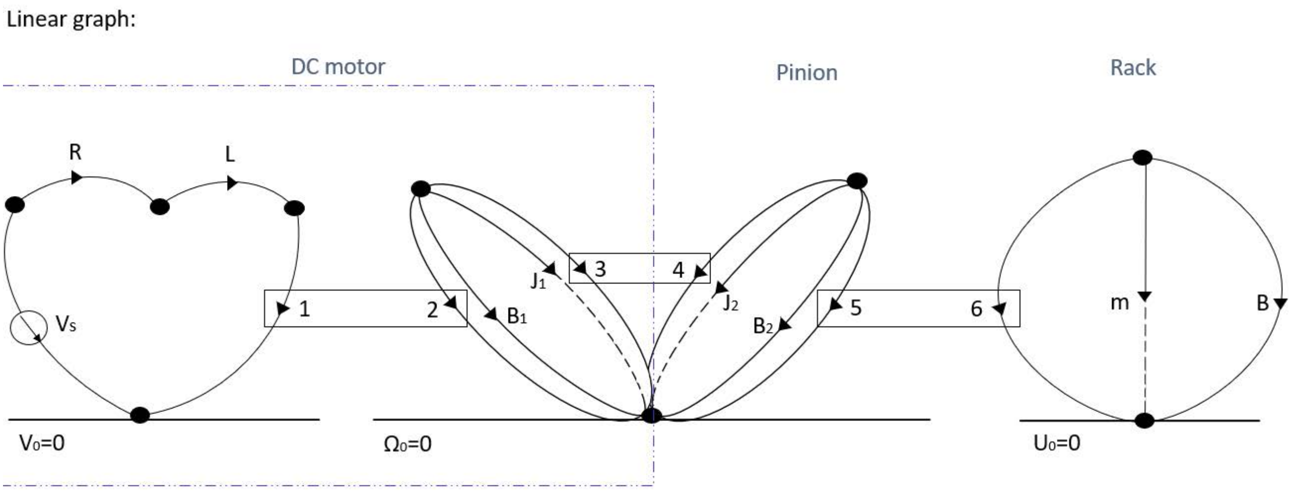

Figure 3.10: Linear graph of DC motor, rack and pinion.

After that step, a normal tree is constructed based on the graph. The tree is a signature of the graph of such a system in order to contain all the nodes of the system graph and to include the maximum number of branches without creating a loop. The normal tree contains initially as much "A" elements as possible, and in the terms of not creating a loop, there can be added dissipative ("D") elements and passive type "T". The branches that are not included in normal tree are the links [15].

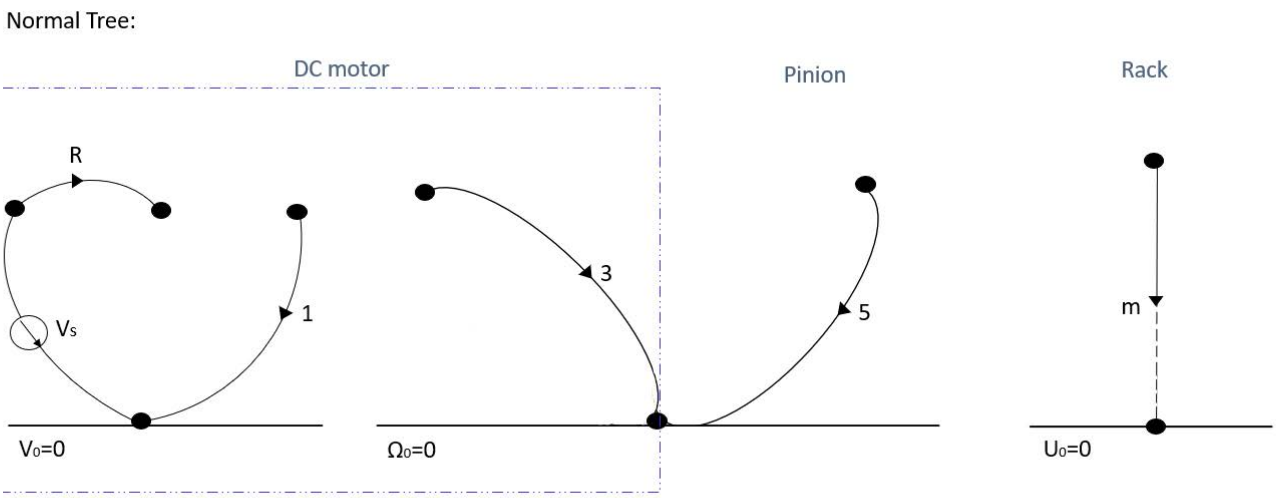

Figure 3.11: Normal tree of DC motor, rack and pinion.

The number of tree links is simply the total number of branches less those in the normal tree [16]:

Number of Branches on the normal tree:

$$B_T = N - 1 \tag{3.8}$$

Number of Branches on the links:

$$B_L = B - B_T = B_N + 1 \tag{3.9}$$

Each time a link is placed in the tree a closed loop is formed, and a compatibility equation may be written for the loop.

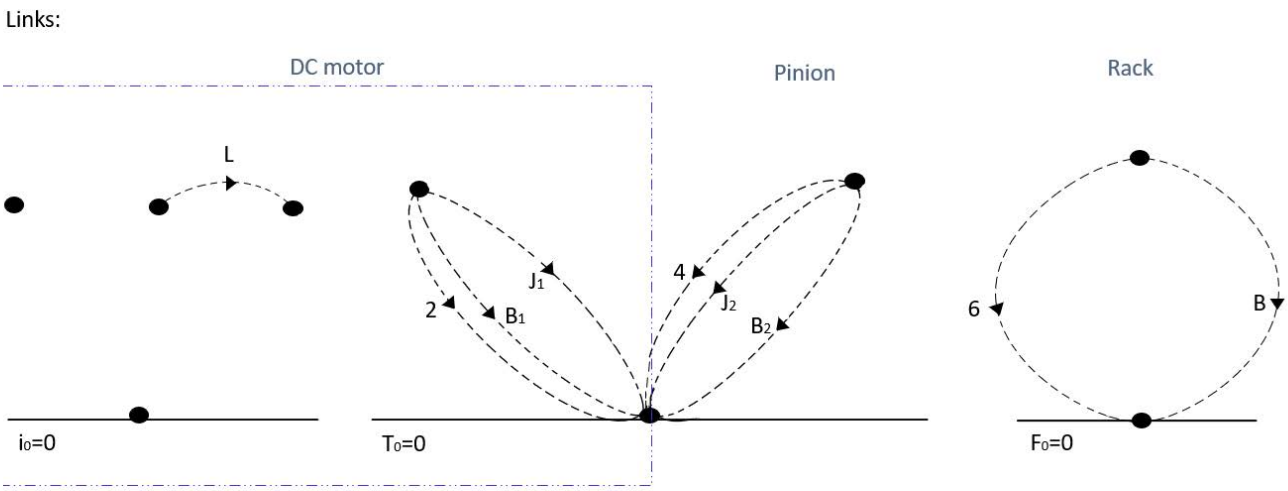

Figure 3.12: Links of DC motor, rack and pinion.

3.2.4 Variables of the system

The variables and parameters of the system that are going to be used to form the equations of the system are given in the table that follows:

V_s	Voltage source
R	Resistance
L	Inductor
V_1	Voltage of electric subsystem of the DC motor
T_2	Torque of the mechanical rotational subsystem of the DC motor
B_1	Coefficient of viscous friction of the two rotational gears of the dc motor
J_1	Inertia of rotational part of the DC motor
Ω_3	angular velocity of the two rotational gears
T_4	Torque of the pinion
J_2	Inertia of the pinion
B_2	Coefficient of viscous friction of the pinion
Ω_5	angular velocity of pinion
F_6	Force that is applied to the system (tube) by the rack
m	Mass of the rack - where U_m is the linear velocity of the mass
B	coefficient of depreciation of the rack

Primary Variables: $V_S, V_R, i_L, V_1, T_2, T_{B_1}, T_{J_1}, \Omega_3, T_4, T_{J_2}, T_{B_2}, \Omega_5, F_6, U_m, F_B$

Secondary Variables: $i_S, i_R, V_L, i_1, \Omega_2, \Omega_{B_1}, \Omega_{J_1}, T_3, \Omega_4, \Omega_{J_2}, \Omega_{B_2}, T_5, U_6, F_m, U_B$

State variables: i_L, U_m

System's Order: 2

Nd : 3

The system's primary variables are the across-elements "A" on tree branches, and the through-elements "T" on the tree links. Conversely, the secondary variables are the through-variables "T" on the tree branches, and the across-variables "A" on tree links [16]. The state variables are the ones that describe the state of the system at a specific time and they form the state equations, a set of differential equations that provide a basis for determining the system's response to external inputs [16]. The system's order is two, due to the number of the independent state variables that define the behavior of the system each time by first-order differential equations for every input. Basically, the system's order is defined as the number of across-variables on the tree and the number of trough-variables on the links. These state variables are usually represented by $x_1, x_2, .., x_n$, where each x represents a different aspect of the system's behavior. The following equations are explained in detail at chapter 3.2.10.

$$\dot{\mathbf{x}} = \mathbf{Ax} + \mathbf{Bu} \tag{3.10}$$

$$\dot{\mathbf{y}} = \mathbf{Cx} + \mathbf{Du} \tag{3.11}$$

Specifically, the system's order defines the dimension of the state vector $\mathbf{x}(\mathbf{t})$. This state vector contains the values of the state variables of the system.

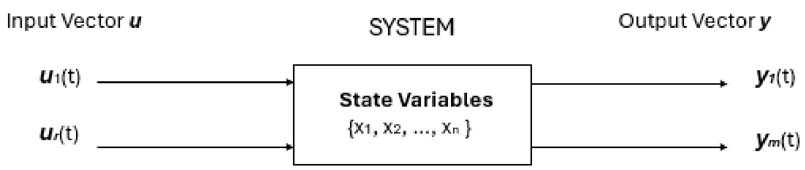

Figure 3.13: Inputs, Outputs and State variables of the system. [15]

The Nd represents the energy domains of the system and in this subsystems they are three: the electrical domain of the DC motor with its mechanical (Rotational) domain together with the one of the pinion, and the Mechanical (Translational) domain of the rack.

3.2.5 Elemental equations of of DC motor and rack-pinion dynamics

The number of elemental equations is defined by this condition:

$$Number\ of\ elemental\ equations = B - S\ (Branches - Sources) \tag{3.12}$$

They relate the through variables "T" with the across variables "A". Each element has its equation that describes it. They represent the fundamental principles-relationships governing the behavior of individual components or elements within a system. More specifically, the elemental equations should have at the left part only primary variables that have been defined above from the graph, and the right part should consist only of secondary ones. In order to eliminate the secondary variables associated with the passive elements of the right part and replace them with primary ones, continuity and compatibility equations, that are going to be formed later, can be used.

$$\frac{di_L}{dt} = \frac{1}{L} \cdot V_L \tag{3.13}$$
$$V_R = i_R \cdot R \tag{3.14}$$
$$T_{B_1} = B_1 \cdot \Omega_{B_1} \tag{3.15}$$
$$T_{B_2} = B_2 \cdot \Omega_{B_2} \tag{3.16}$$
$$T_{J_1} = J_1 \cdot \frac{d\Omega_{J_1}}{dt} \tag{3.17}$$
$$T_{J_2} = J_2 \cdot \frac{d\Omega_{J_2}}{dt} \tag{3.18}$$
$$V_1 = -Kt \cdot \Omega_2 \tag{3.19}$$
$$T_2 = Kt \cdot i_1 \tag{3.20}$$
$$\Omega_3 = -n \cdot \Omega_4 \tag{3.21}$$
$$T_4 = n \cdot T_3 \tag{3.22}$$
$$\Omega_5 = \frac{1}{\rho} \cdot U_6 \tag{3.23}$$
$$F_6 = -\frac{1}{\rho} \cdot T_5 \tag{3.24}$$
$$\frac{dU_m}{dt} = \frac{1}{m} \cdot F_m \tag{3.25}$$
$$F_B = B \cdot U_B \tag{3.26}$$

3.2.6 Continuity equations of of DC motor and rack-pinion dynamics

The continuity equations represent a set of through-variables passing through any closed contour/node on the graph. The basic rule of the continuity is that the sum of the through variables on the graph that cross a node equals to zero. Specifically, they are the sum of the through "T" variables that cross each node and their sign is based on whether the components are entering or leaving the node.The inherent understanding is that the variable T does not accumulate at a single node, as a node typically denotes a point rather than an accumulation site for the integrated variable T (e.g. electric charge accumulation). If accumulation were to occur at a node, it would transform the node into an accumulation element "A", which is not feasible [15]. Equivalently written:

$$\sum_{i=1}^{N} f_i = 0 \tag{3.27}$$

The image in Figure 3.14 provides an example illustrating the fulfillment of the continuity condition. Negative signs are present in the variables as they exit the node:

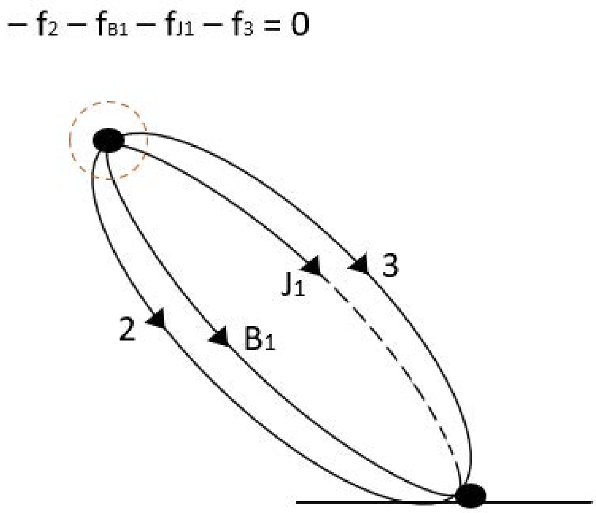

Figure 3.14: Representation of continuity at a node.

The number of these equations is defined by the following mathematical type:

$$N - Nd - S_A = 9 - 3 - 1 = 5 \tag{3.28}$$

where N is the number of all the nodes, Nd is the number of the energy domains that exist in the system and S_A is the number of the across sources "A". If a closed contour is drawn on a tree such that it cuts only one tree branch, then the through-variable on that branch (a secondary variable), may be expressed in terms of the through-variables on tree links, which are primary variables. Based on this system's graph, the continuity equations that describe the system are:

$$T_3 = -T_{J_1} - T_{B_1} - T_2 \tag{3.29}$$

$$i_R = i_L \tag{3.30}$$

$$i_1 = i_L \tag{3.31}$$

$$T_5 = -T_4 - T_{J_2} - T_{B_2} \tag{3.32}$$

$$F_m = -F_6 - F_B \tag{3.33}$$

3.2.7 Compatibility equations of of DC motor and rack-pinion dynamics

The compatibility constraint equations relate across-variables "A" around any closed loop in the system graph. The basic rule of the compatibility is that the sum of the across power variables of branches along a closed loop equals zero. Each time a link is placed in the tree a closed loop is formed, and a compatibility equation may be written for the loop. The sign of the term U_i in the sum is determined by the direction of the arrow of the corresponding branch, which indicates the direction of the "fall" of the value U_i along the branch. Equivalently written:

$$\sum_{i=1}^{N} U_i = 0 \tag{3.34}$$

The image in Figure 3.15 illustrates an example demonstrating the fulfillment of compatibility conditions. n this equation, only across variables 'A' are used because this procedure occurs in the normal tree, where only across "A" variables are present. After adding a branch from links in the normal tree and determining the positive direction of the system, a check is performed for closed loops, leading to the formation of compatibility equations.

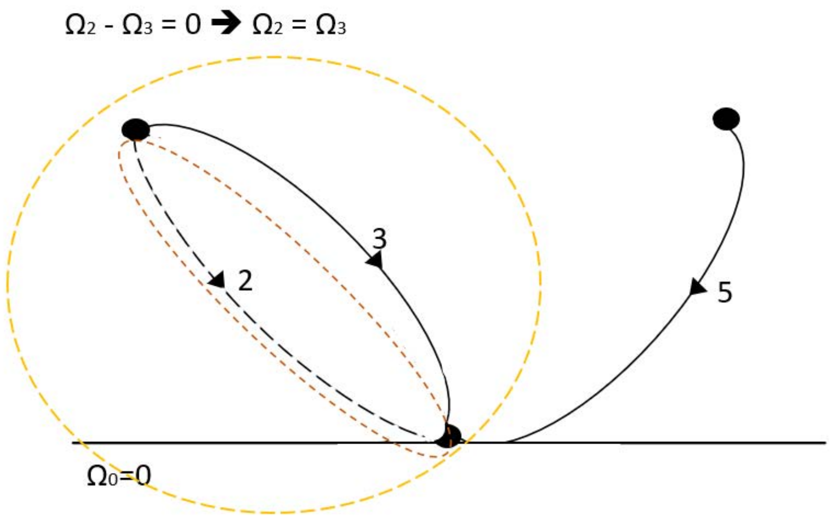

Figure 3.15: Representation of compatibility in a closed loop.

The number of these equations is defined by the following calculation:

$$B - N + Nd - S_T = 15 - 9 + 3 = 9 \tag{3.35}$$

where B is the number of branches, N is the number of nodes, Nd is the number of the energy domains that exist in the system and ST is the number of the through sources "T". In general, each time a loop is formed by placing a link in a tree, the across-variable on that link may be written in terms of the across-variables on the tree branches. The resulting compatibility equation contains only one secondary variable at the left side and primaries at the right one [16]. Based on the graph, the compatibility equations that describe the system are:

$$\begin{aligned} V_S &= V_R + V_L + V_1 \\ \Rightarrow V_L &= V_S - V_R - V_1 \end{aligned} \tag{3.36}$$

$$\Omega_{J_1} = \Omega_3 \tag{3.37}$$

$$\Omega_{B_1} = \Omega_3 \tag{3.38}$$

$$\Omega_2 = \Omega_3 \tag{3.39}$$

$$\Omega_{B_2} = \Omega_5 \tag{3.40}$$

$$\Omega_{J_2} = \Omega_5 \tag{3.41}$$

$$\Omega_4 = \Omega_5 \tag{3.42}$$

$$U_B = U_m \tag{3.43}$$

$$U_6 = U_m \tag{3.44}$$

$$\tag{3.45}$$

The resulting equations that retrieved from above and are going to be used later are:

$$\Omega_3 = -n \cdot \Omega_5 \Rightarrow \Omega_3 = -n \cdot \frac{1}{\rho} \cdot U_m \tag{3.46}$$

$$\Omega_5 = \frac{1}{\rho} \cdot U_m \tag{3.47}$$

3.2.8 Final elemental equations after substitution

The elemental equations should consist of primary variables only. The secondary variables are going to be replaced with primaries of the above continuity and compatibility equations. The **final elemental equations** are the following:

$$\frac{di_L}{dt} = \frac{1}{L} \cdot V_L \tag{3.48}$$

$$\Rightarrow \frac{di_L}{dt} = \frac{1}{L} \cdot (V_S - V_R - V_1) \tag{3.49}$$

$$V_R = i_R \cdot R \tag{3.50}$$

$$\Rightarrow V_R = i_L \cdot R \tag{3.51}$$

$$T_{B_1} = B_1 \cdot \Omega_{B_1} \tag{3.52}$$

$$\Rightarrow T_{B_1} = B_1 \cdot \Omega_3 \tag{3.53}$$

$$T_{B_2} = B_2 \cdot \Omega_{B_2} \tag{3.54}$$

$$\Rightarrow T_{B_2} = B_2 \cdot \Omega_5 \tag{3.55}$$

$$T_{J_1} = J_1 \cdot \frac{d\Omega_{J_1}}{dt} \tag{3.56}$$

$$\Rightarrow T_{J_1} = J_1 \cdot \frac{d\Omega_3}{dt} \tag{3.57}$$

$$T_{J_2} = J_2 \cdot \frac{d\Omega_{J_2}}{dt} \tag{3.58}$$

$$\Rightarrow T_{J_2} = J_2 \cdot \frac{d\Omega_5}{dt} \tag{3.59}$$

$$V_1 = -Kt \cdot \Omega_2 \tag{3.60}$$

$$\Rightarrow V_1 = -Kt \cdot \Omega_3 \tag{3.61}$$

$$T_2 = Kt \cdot i_1 \tag{3.62}$$

$$\Rightarrow T_2 = Kt \cdot i_L \tag{3.63}$$

$$\Omega_3 = -n \cdot \Omega_4 \tag{3.64}$$

$$\Rightarrow \Omega_3 = -n \cdot \Omega_5 \tag{3.65}$$

$$T_4 = n \cdot T_3 \tag{3.66}$$

$$\Rightarrow T_4 = n \cdot (-T_{J_1} - T_{B_1} - T_2) \tag{3.67}$$

$$\tag{3.68}$$

$$\Omega_5 = \frac{1}{\rho} \cdot U_6 \tag{3.69}$$

$$\Rightarrow \Omega_5 = \frac{1}{\rho} \cdot U_m \tag{3.70}$$

$$F_6 = -\frac{1}{\rho} \cdot T_5 \tag{3.71}$$

$$= -\frac{1}{\rho} \cdot (-T_4 - T_{J_2} - T_{B_2}) \tag{3.72}$$

$$= \frac{1}{\rho} \cdot (T_4 + T_{J_2} + T_{B_2}) \tag{3.73}$$

$$\Rightarrow F_6 = \frac{1}{\rho} \cdot (T_4 + T_{J_2} + T_{B_2}) \tag{3.74}$$

$$\frac{dU_m}{dt} = \frac{1}{m} \cdot F_m \tag{3.75}$$

$$= -\frac{1}{m} \cdot (F_6 + F_B) \tag{3.76}$$

$$\Rightarrow \frac{dU_m}{dt} = -\frac{1}{m} \cdot (F_6 + F_B) \tag{3.77}$$

$$F_B = B \cdot U_B \tag{3.78}$$

$$\Rightarrow F_B = B \cdot U_m \tag{3.79}$$

3.2.9 State equations of DC motor and rack-pinion dynamics

The differential state equations describe how the system's state variables change over time based on the system's inputs and internal dynamics and are expressed in terms of a set of state variables. Specifically, these equations express the derivatives of the state variables directly in terms of the state variables and the input. These equations are derived by substituting all secondary variables into the final elemental equations of state variables, expressing them as functions of the remaining state variables and including also the system's inputs. For the system that is studied in this chapter, the final state equations are the following:

$$\begin{aligned}
\frac{di_L}{dt} &= \frac{1}{L}\cdot(V_S - V_R - V_1) = \frac{1}{L}\cdot(V_S - i_L\cdot R - (-Kt\cdot\Omega_3)) \\
&= \frac{1}{L}\cdot(V_S - i_L\cdot R + Kt\cdot\Omega_3) = \frac{1}{L}\cdot(V_S - i_L\cdot R + Kt\cdot(-n\cdot\Omega_5)) \\
&= \frac{1}{L}\cdot\left(V_S - i_L\cdot R + Kt\cdot\left(-n\cdot\frac{1}{\rho}\cdot U_m\right)\right) \\
&= \frac{1}{L}\cdot\left(V_S - i_L\cdot R - n\cdot Kt\cdot\frac{1}{\rho}\cdot U_m\right) \\
\Rightarrow \frac{di_L}{dt} &= \frac{1}{L}\cdot\left(V_S - i_L\cdot R - n\cdot Kt\cdot\frac{1}{\rho}\cdot U_m\right) \qquad (3.80) \\
\frac{dU_m}{dt} &= -\frac{1}{m}\cdot(F_6 + F_B) \\
\Rightarrow \frac{dU_m}{dt} &= -\frac{1}{m}\cdot(F_6 + B\cdot U_m) \qquad (3.81)
\end{aligned}$$

From elemental equation (3.74):

$$\begin{aligned}
F_6 &= -\frac{1}{\rho}\cdot T_5 = \frac{1}{\rho}\cdot(T_4 + T_{J_2} + T_{B_2}) \\
&= \frac{1}{\rho}\cdot[n\cdot(-T_{J_1} - T_{B_1} - T_2) + T_{J_2} + T_{B_2}] \\
&= \frac{1}{\rho}\cdot[n\cdot\left(-J_1\cdot\frac{d\Omega_3}{dt} - B_1\cdot\Omega_3 - Kt\cdot i_L\right) + J_2\cdot\frac{d\Omega_5}{dt} + B_2\cdot\Omega_5] \\
&= \frac{1}{\rho}\cdot[n\cdot\left(-J_1\cdot\frac{d\left(-n\cdot\frac{1}{\rho}\cdot U_m\right)}{dt} - B_1\cdot\left(-n\cdot\frac{1}{\rho}\cdot U_m\right) - Kt\cdot i_L\right) \\
&\quad + J_2\cdot\frac{d\left(\frac{1}{\rho}\cdot U_m\right)}{dt} + B_2\cdot\frac{1}{\rho}\cdot U_m] \\
&= \frac{1}{\rho}\cdot[n\left(J_1\cdot n\cdot\frac{1}{\rho}\cdot\frac{dU_m}{dt} + B_1\cdot n\cdot\frac{1}{\rho}\cdot U_m - Kt\cdot i_L\right) \\
&\quad + J_2\cdot\frac{1}{\rho}\cdot\frac{dU_m}{dt} + B_2\cdot\frac{1}{\rho}\cdot U_m] \\
&= \frac{1}{\rho}\cdot[n^2\cdot\frac{1}{\rho}\cdot J_1\cdot\frac{dU_m}{dt} + n^2\cdot\frac{1}{\rho}\cdot B_1\cdot U_m - n\cdot Kt\cdot i_L \\
&\quad + J_2\cdot\frac{1}{\rho}\cdot\frac{dU_m}{dt} + B_2\cdot\frac{1}{\rho}\cdot U_m]
\end{aligned}$$

$$\begin{aligned}
&= n^2\cdot\frac{1}{\rho^2}\cdot J_1\cdot\frac{dU_m}{dt} + n^2\cdot\frac{1}{\rho^2}\cdot B_1\cdot U_m - \frac{1}{\rho}\cdot n\cdot Kt\cdot i_L \\
&\quad + \frac{1}{\rho^2}\cdot J_2\cdot\frac{dU_m}{dt} + \frac{1}{\rho^2}\cdot B_2\cdot U_m \\
&= \frac{dU_m}{dt}\left(\frac{1}{\rho^2}\cdot\left(n^2\cdot J_1 + J_2\right)\right) + U_m\left(\frac{1}{\rho^2}\cdot\left(n^2\cdot B_1 + B_2\right)\right) - \frac{1}{\rho}\cdot n\cdot Kt\cdot i_L \\
\Rightarrow F_6 &= \frac{dU_m}{dt}\left(\frac{1}{\rho^2}\cdot\left(n^2\cdot J_1 + J_2\right)\right) + U_m\left(\frac{1}{\rho^2}\cdot\left(n^2\cdot B_1 + B_2\right)\right) - \frac{1}{\rho}\cdot n\cdot Kt\cdot i_L
\end{aligned}$$

From the state equation (3.81) based on the result of (3.82):

$$\frac{dU_m}{dt} = -\frac{1}{m}\cdot(F_6+F_B) = -\frac{1}{m}\cdot(F_6+B\cdot U_m)$$
$$= -\frac{1}{m}\cdot\Bigg(n^2\cdot\frac{1}{\rho^2}\cdot J_1\cdot\frac{dU_m}{dt}+n^2\cdot\frac{1}{\rho^2}\cdot B_1\cdot U_m-\frac{1}{\rho}\cdot n\cdot Kt\cdot i_L+\frac{1}{\rho^2}\cdot J_2\cdot\frac{dU_m}{dt}$$
$$+\frac{1}{\rho^2}\cdot B_2\cdot U_m+B\cdot U_m\Bigg)$$
$$\Rightarrow \frac{dU_m}{dt} = -\frac{1}{m}\cdot[\frac{dU_m}{dt}\left(\frac{1}{\rho^2}\cdot\left(n^2\cdot J_1+J_2\right)\right)+U_m\cdot\left(\frac{1}{\rho^2}\left(n^2\cdot B_1+B_2\right)+B\right)$$
$$-\frac{1}{\rho}\cdot n\cdot Kt\cdot i_L]$$
$$\Rightarrow \frac{dU_m}{dt}+\frac{dU_m}{dt}\cdot\left(\frac{\frac{1}{\rho^2}\cdot(n^2\cdot J_1+J_2)}{m}\right) = -\frac{U_m\cdot\frac{n^2\cdot B_1+B_2}{\rho^2}}{m}+\frac{i_L\cdot\frac{n\cdot Kt}{\rho}}{m}$$
$$\Rightarrow\frac{dU_m}{dt}\left(1+\frac{\frac{n^2\cdot J_1+J_2}{\rho^2}}{m}\right) = -\frac{U_m\frac{n^2\cdot B_1+B_2+\rho^2\cdot B}{\rho^2}}{m}+\frac{i_l\cdot\frac{n\cdot Kt}{\rho}}{m}$$
$$\Rightarrow\frac{dU_m}{dt}\left(\frac{m+\frac{n^2\cdot J_1+J_2}{\rho^2}}{m}\right) = -\frac{U_m\frac{n^2\cdot B_1+B_2+\rho^2\cdot B}{\rho^2}}{m}+\frac{i_l\cdot\frac{n\cdot Kt}{\rho}}{m}$$
$$\Rightarrow\frac{dU_m}{dt}\left(\frac{\rho^2\cdot m+n^2\cdot J_1+J_2}{\rho^2}\right) = -U_m\cdot\frac{n^2\cdot B_1+B_2+\rho^2\cdot B}{\rho^2}+i_L\cdot\frac{n\cdot Kt}{\rho}$$
$$\Rightarrow\frac{dU_m}{dt} = \frac{-U_m\cdot\frac{n^2\cdot B_1+B_2+\rho^2\cdot B}{\rho^2}}{\frac{\rho^2\cdot m+n^2\cdot J_1+J_2}{\rho^2}}+\frac{i_L\cdot\frac{n\cdot Kt}{\rho}}{\frac{\rho^2\cdot m+n^2\cdot J_1+J_2}{\rho^2}}$$
$$\Rightarrow\frac{dU_m}{dt} = -U_m\cdot\frac{n^2\cdot B_1+B_2+\rho^2\cdot B}{\rho^2\cdot m+n^2\cdot J_1+J_2}+i_L\cdot\frac{n\cdot Kt\cdot\rho}{\rho^2\cdot m+n^2\cdot J_1+J_2} \tag{3.82}$$

The final state equations of the system are:

$$\frac{di_L}{dt} = \frac{1}{L}\cdot\left(V_S-i_L\cdot R-n\cdot Kt\cdot\frac{1}{\rho}\cdot U_m\right) \tag{3.83}$$
$$\frac{dU_m}{dt} = -U_m\cdot\frac{n^2\cdot B_1+B_2+\rho^2\cdot B}{\rho^2\cdot m+n^2\cdot J_1+J_2}+i_L\cdot\frac{n\cdot Kt\cdot\rho}{\rho^2\cdot m+n^2\cdot J_1+J_2} \tag{3.84}$$

3.2.10 Matrix formulation

The complete system model for a linear time-invariant system consists of a set of n state equations, defined in terms of the matrices A and B, and a set of output equations that relate any output variables of interest to the state variables and inputs, and expressed in terms of the **C** and **D** matrices [15]:

$$\mathbf{y} = \mathbf{C}\mathbf{x} + \mathbf{D}\mathbf{u} \tag{3.85}$$

The **y** variable each time depends on the elements that is needed to be measured as output. The state equations in terms of the elements should be written in a matrix in the form of

$$\dot{\mathbf{x}} = \mathbf{A}\mathbf{x} + \mathbf{B}\mathbf{u} \tag{3.86}$$

where: **x** is the state-vector and is given by

$$\mathbf{x} = \begin{bmatrix} i_L \\ U_m \end{bmatrix} \tag{3.87}$$

A is the system matrix given by

$$\mathbf{A} = \begin{bmatrix} -\frac{R}{L} & -\frac{n \cdot Kt}{\rho \cdot L} \\ \frac{n \cdot Kt \cdot \rho}{\rho^2 \cdot m + n^2 \cdot J_1 + J_2} & -\frac{n^2 \cdot B_1 + B_2 + \rho^2 \cdot B}{\rho^2 \cdot m + n^2 \cdot J_1 + J_2} \end{bmatrix} \tag{3.88}$$

Its dimensions are defined by the number of the state variables of the system. It describes the interaction of the system's state variables. Specifically, the element a_{11} is given by

$$a_{11} = -\frac{R}{L} \tag{3.89}$$

and represents the effect of i_L on its own rate of change. The element a_{12} is given by

$$a_{12} = -\frac{n \cdot Kt}{\rho \cdot L} \tag{3.90}$$

and represents the effect of $U_m$on the rate of change of i_L. Similarly, the element a_{21} is given by

$$a_{21} = \frac{n \cdot Kt \cdot \rho}{\rho^2 \cdot m + n^2 \cdot J_1 + J_2} \tag{3.91}$$

and represents the effect of i_L on the rate of change of U_m. The the element a_{22} is given by

$$a_{22} = \frac{n^2 \cdot B_1 + B_2 + \rho^2 \cdot B}{\rho^2 \cdot m + n^2 \cdot J_1 + J_2} \tag{3.92}$$

and represents the effect of U_m on its own rate of change. The input matrix **B** is given by

$$\mathbf{B} = \begin{bmatrix} \frac{1}{L} \\ 0 \end{bmatrix} \tag{3.93}$$

and relates the system inputs to the state variables **x**. Vector **u** represents the input vector, which is in this case is a scalar given by the voltage source V_S

$$\mathbf{u} = V_s \tag{3.94}$$

Specifically, the matrices are formed like this:

$$\frac{d}{dt}\begin{bmatrix} i_L \\ U_m \end{bmatrix} = \begin{bmatrix} -\frac{R}{L} & -\frac{Kt\cdot n}{\rho\cdot L} \\ \frac{n\cdot Kt\cdot \rho}{\rho^2\cdot m+n^2\cdot J_1+J_2} & -\frac{n^2\cdot B_1+B_2+\rho^2\cdot B}{\rho^2\cdot m+n^2\cdot J_1+J_2} \end{bmatrix} \cdot \begin{bmatrix} i_L \\ U_m \end{bmatrix} + \begin{bmatrix} \frac{1}{L} \\ 0 \end{bmatrix} \cdot V_s \tag{3.95}$$

3.3 Simulation results

The provided MATLAB code simulates the behavior of a DC motor with rack and pinion dynamics and plots the linear velocity and current over time. The simulation results are shown in the two following images3.16 3.17. In order to solve the nonstiff differential equations (state equations) that arose by this system, there was used a numerical solver from MATLAB:function ODE45. This function implements a Runge-Kutta method with a variable time step for efficient computation.This solver is particularly useful for nonstiff ODEs, where the solution changes relatively slowly and stiffness is not a concern. Based on the step, it calculates the integration for this specific step, and by this way it represents the solution over time [20].

```
%motor.m        %file name
% MATLAB code to plot the behavior of the DC motor with rack and
   pinion dynamics
%ode45 dc motor function
parameters_integration;

tspan=[0 1];
y0=[0 0];

options = odeset('RelTol', reltol, 'AbsTol',abstol,...
            'MaxStep',maxstep, 'InitialStep', initstep);
[t,y]=ode45(@(t,y)DCMOTOR(t,y),tspan,y0, options);

%plot linear velocity
figure(1);
plot(t,y(:,1))
xlabel('time [sec]')
ylabel('linear velocity [m/sec]')

%plot current
figure(2);
plot(t,y(:,2))
xlabel('time [sec]')
ylabel('current [A]')


function dydt=DCMOTOR(t,y)
```

```
    maxon_parameters_DCX_35;

    dydt = zeros(2,1); %initialize the table with zeros
    y1=y(1); %iL - current
    y2=y(2); %Um - velocity

    %state equations of the system
    %diL/dt:
    dydt1=(-R/L)*y1-(n*Kt/radius*L)*y2+Vs/L;
    %dUm/dt:
    dydt2=((n*Kt*radius)*y1-((n^2)*B1+B2+(radius^2)*B)*y2)/((radius^2)
        *m+(n^2)*J1+J2);

    dydt=[dydt1; dydt2]; %array where the solutions of integration of
        each state equation are stored
end
```

The files that were used with the initialized parameters for the ODE45 and for the motor with the rack and pinion are the following:

```
%parameters_integration.m    %file name

    % parameters of the ODE45
    reltol = 1e-3;    %desired accuracy - relative tolerance
    abstol = [1e-2 1e-2]; %maximum permissible error - absolute
        tolerance
    maxstep = 1e-2;  %maximum allowed step size during the integration
         process.
    initstep = 0.001; % initial step size used by the solver at the
        start of the integration process.
    %It helps the solver to adapt its step size based on the behavior
        of the solution
```

```
%maxon_parameters_DCX_35.m     %file name
%DCX 35 L 35 mm, Graphite Brushes, ball bearings

  radius = 5*10^(-2); %m -- of the pinion
  n = 1;
  J1 = 9.95*10^(-6); %kg*m^2 -- of the dc motor
  J2 = (1/2)*(200*10^(-3))*(5*10^(-2))^2; %(1/2)*m*r^2 -- inertia of
     the pinion
```

```
m = 200*10^(-2); %kg -- mass of the rack
R = 0.0788; % terminal resistance
L = 0.0263*10^(-3); %H terminal inductance
Kt = 13.7*10^(-3);
tconstant = 4.21*10^(-3); %Sec
B2 = 0.1; %of the pinion

Vs = 12; %source
i_nl = 320*10^(-3); %no load current
w_nl = 8130*2*pi*60; %rpm (rads per minute) -- no load
B1 = i_nl/w_nl * Kt;  %viscous friction of the dc motor
B = 0.2;
```

In the following figure 3.16 is represented the output of the integration of the state equation of coil's current and illustrates the value of current of the dc motor over time (for 1 second) until it reaches a steady state value (1 Amber). The current plot shows a transient response where the current quickly rises to approximately 1 A and then stabilizes. The ups and down of the plot's line represent the continuous motion of the dc motor that provides the current. This behavior is typical of a DC motor where the initial current surge occurs due to the inrush current required to overcome the inertia of the system and start the motion. Once the motor reaches a steady state, the current stabilizes as it only needs to overcome the steady-state frictional forces.

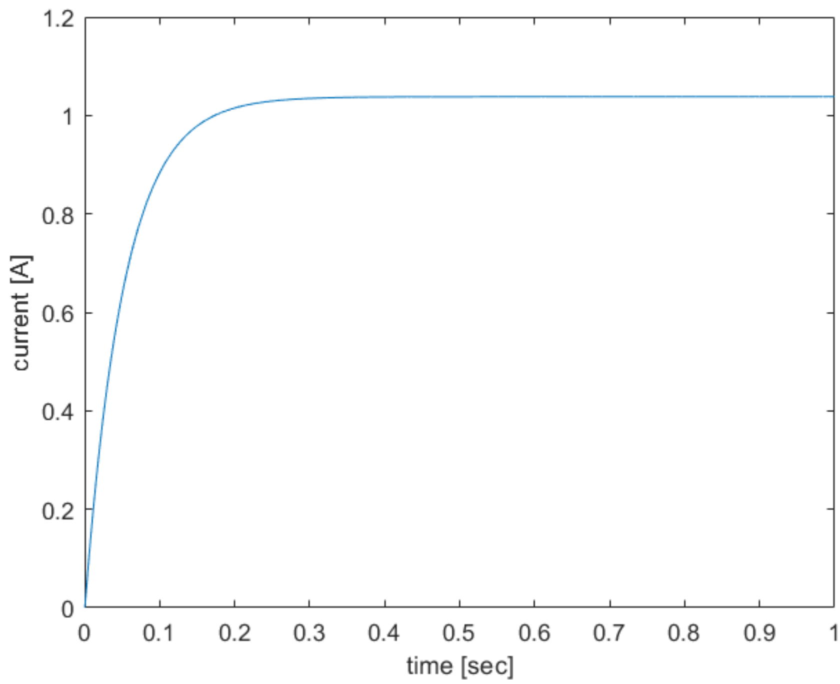

Figure 3.16: Current of DC Motor.

The linear velocity plot 3.17 shows a similar transient response where the velocity quickly rises to around 150 m/sec and then stabilizes. This rapid increase represents the motor accelerating the rack until it reaches a steady-state speed. The stabilization indicates that the forces (torque) provided by the motor balance out with the frictional forces in the system.

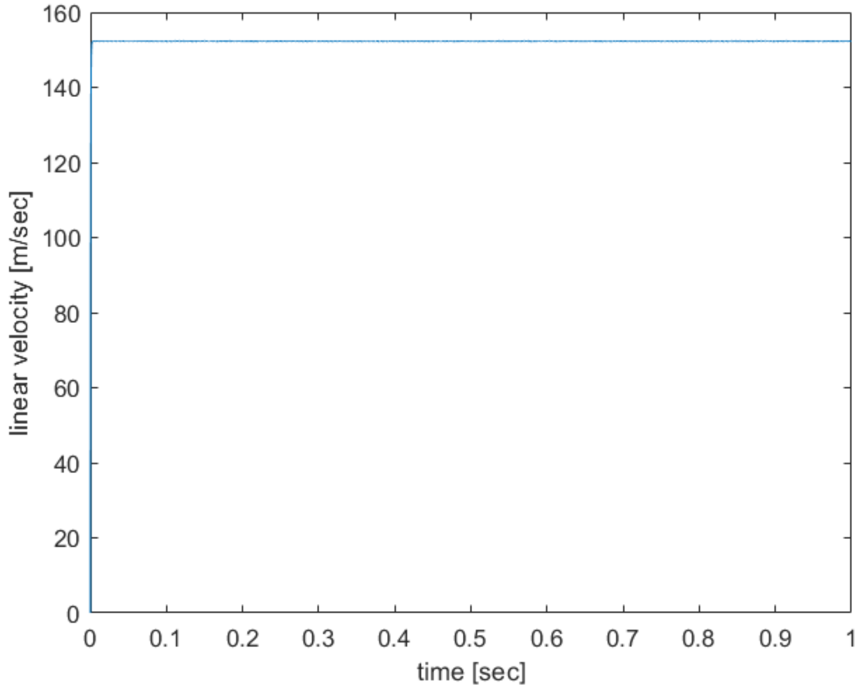

Figure 3.17: Linear velocity of the DC motor.

3.4 Conclusions

In this chapter, the system that was examined and analyzed was the DC motor with rack and pinion dynamics. Modeling techniques were employed to develop linear graphs, normal trees, and links. The variables describing the system's dynamics were classified, resulting in the formation of equations for elements, continuity, stability, and state. The state equations, which describe the system's behavior at specific times, were derived from these foundational equations. Following this, matrices that describe the system's output were also constructed, providing a comprehensive representation of the system's dynamics. Furthermore, the Two-Port Energy Transducing Elements were studied, specifically Transformers, that convert energy from one domain to another. These elements involve variables known as power variables, as their multiplication yields the system's power.
Afterward, these equations were implemented in Matlab to simulate and integrate the system. Through this integration, the state variables could be examined when plotted.

The plot of the current indicated a rapid rise to 1 ampere before stabilizing. This behavior is typical, with the initial surge due to inrush current overcoming system inertia, followed by stabilization as steady-state frictional forces are balanced. Similarly, the linear velocity plot shows the velocity rising to around 150 m/sec before stabilizing, indicating the motor's acceleration of the rack until a steady-state speed is achieved.

Chapter 4

Modeling of eversion system and of complete system

4.1 Introduction

In this chapter, the whole system is going to be modeled and analyzed, with special emphasis on the new addition: the growing element that is inside the pressurization tank. As the active channel moves to the right direction, the growing element starts moving with the same velocity as the active channel, the everting begins and the growing element comes out from the pressurization tank.

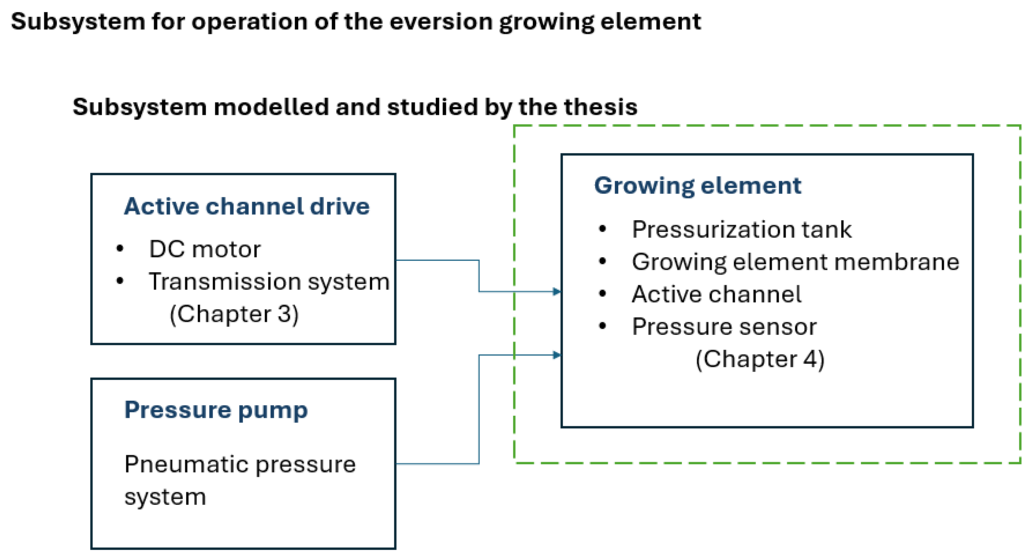

Figure 4.1: System's architecture that is going to be studied in this chapter.

The architecture of the entire system, with special emphasis on the internal components of the growing element, is depicted in Figure 4.2. This system will be represented as a dynamic model. A graph will be constructed, and the state equations for the entire system will be formulated. Additionally, a MATLAB code will be developed to simulate the system's behavior and present the results in chapter4.4.

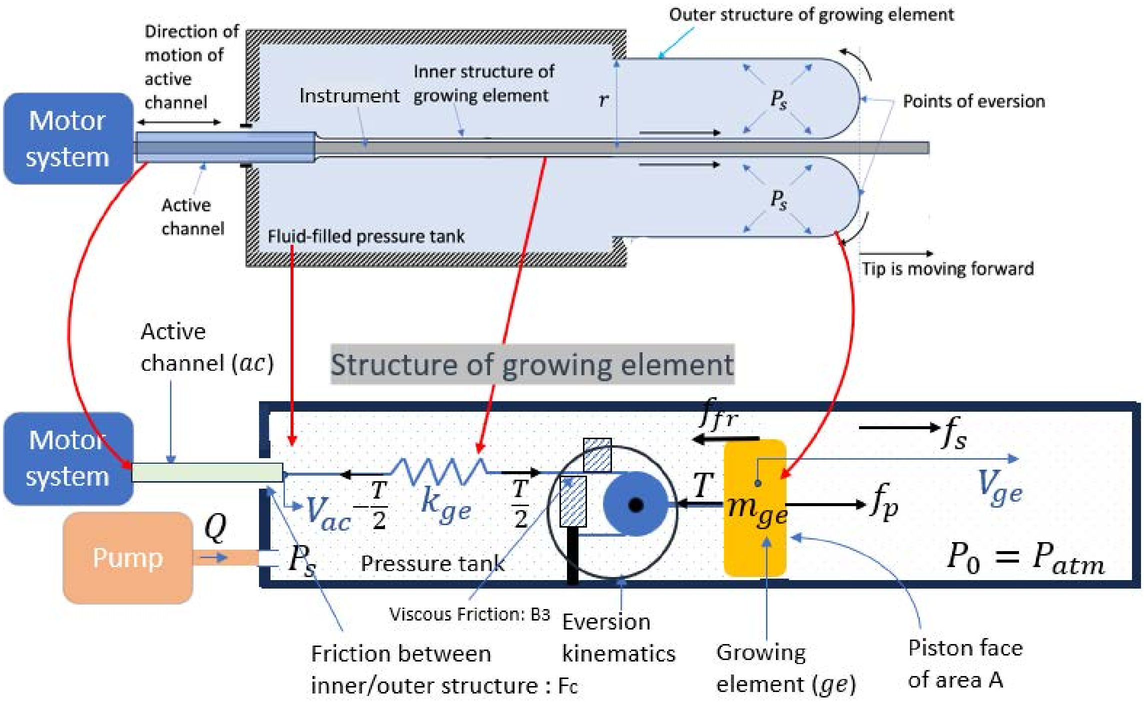

Figure 4.2: Growing element's architecture inside the pressurization tank [14].

In this section, the rack described in the previous chapter is now attached to the active channel, which in turn is connected to the growing element with a spring. The active channel and the rack will be considered as one mass. The active channel's linear velocity is derived from the transformation of the rotational velocity of the pinion (with the usage of the transformer). The friction that occurs in the growing element is viscous friction (B_3) due to the fluid environment. Additionally, between the surface of the active channel and the growing element, a static force occurs, which is represented in the graph as a Coulomb friction source (F_c). The pressurization tank is modeled as a pressure source (P_S) with fluid resistance (R_f). This system is connected to the growing element through a gyrator.

4.2 Mathematical model

4.2.1 Two-Port Energy Transducing Elements - Gyrators

In order to transduce hydraulic energy into mechanical, or the opposite, the type of transducer that is going to be used is called gyrator. Gyrators are described by the following algebraic expressions:

$$u_1 = GY \cdot f_2 \tag{4.1}$$
$$f_1 = -\frac{1}{GY} \cdot u_2 \tag{4.2}$$

where u_i (i = 1,2) are variables of type "A", f_i (i = 1,2) are variables of type "T" and GY the gyrator parameter. Therefore, a gyrator algebraically connects variable type "A" with variable of type "T" and the opposite. Equation 4.2 states that the across-variable u_1 is related by a constant, GY , to the through-variable f_2, and the through-variable f_1 is related by the negative reciprocal constant $\frac{1}{GY}$ to the across-variable u_2 [17]. In matrix form, the equations governing a gyrator are written as follows:

$$\begin{bmatrix} u_1(t) \\ f_1(t) \end{bmatrix} = \begin{bmatrix} 0 & GY \\ -\frac{1}{GY} & 0 \end{bmatrix} \cdot \begin{bmatrix} u_2(t) \\ f_2(t) \end{bmatrix} \tag{4.3}$$

4.2.2 Linear Graph, Normal Tree and Links formulation

The linear graph representing the entire everting system -including the DC motor, rack and pinion dynamics, the active channel connected to the growing element, and the pressurization tank- is shown in the following figure 4.3. The subsystem that was analyzed in the previous chapter remains the same. The addition is the graph of the active channel, of the growing element and of the pressurization tank. The Coulomb's friction in the growing element is represented as a source because it isn't correlated somehow with the node that represents the velocity of the growing element U_{ge}. Friction in this context is directly proportional to the mass of the growing element and acts in the direction towards the ground. For sources of type "T", the arrow direction starts from the node with the maximum value and points towards the node with the minimum value, in contrast to type "A" sources. The active channel is connected to the growing element via a spring, allowing the growing element to move through oscillations while maintaining a secure connection that prevents breakage. The spring controls these oscillations and strives to maintain a constant distance between the active channel and the growing element. The growing element is connected to the pressurization tank via a gyrator, which converts mechanical energy into hydraulic energy.

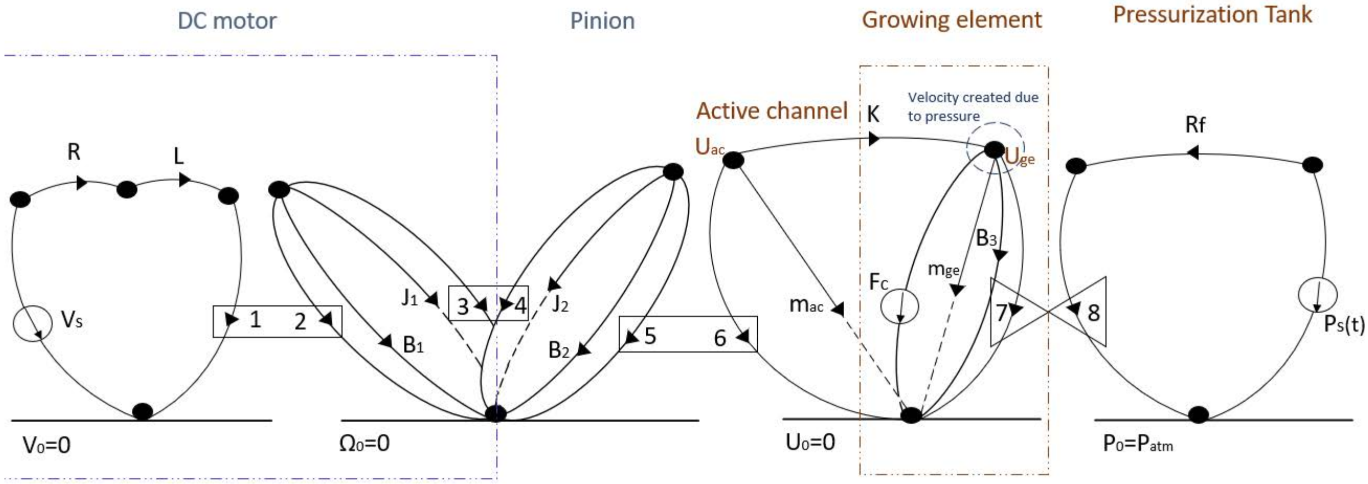

Figure 4.3: Linear graph of eversion system and of complete system.

Normal Tree:

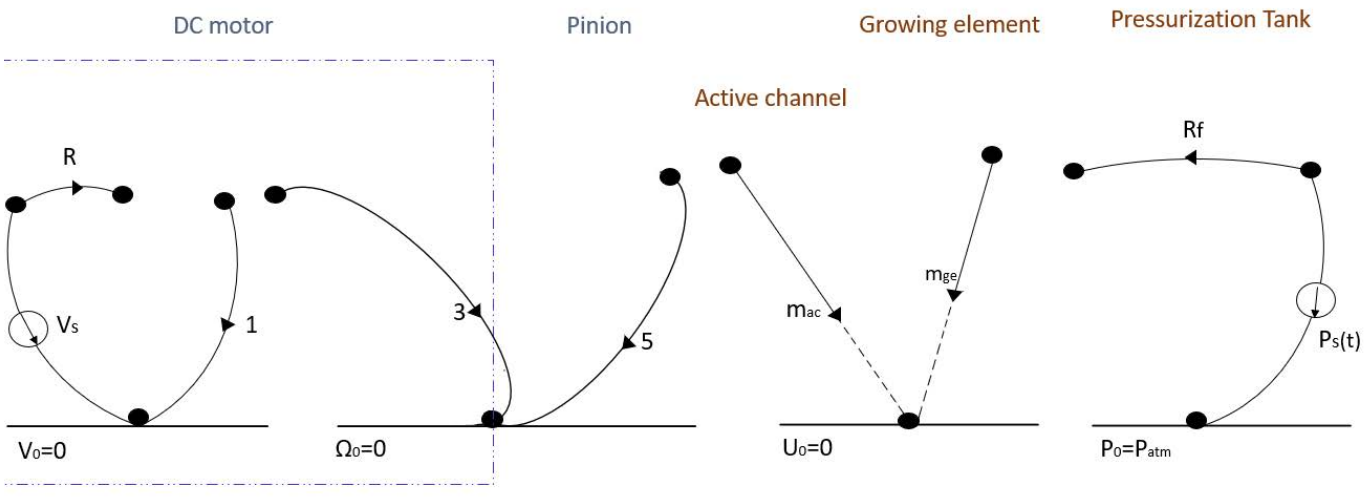

Figure 4.4: Normal Tree of eversion system and of complete system.

Links:

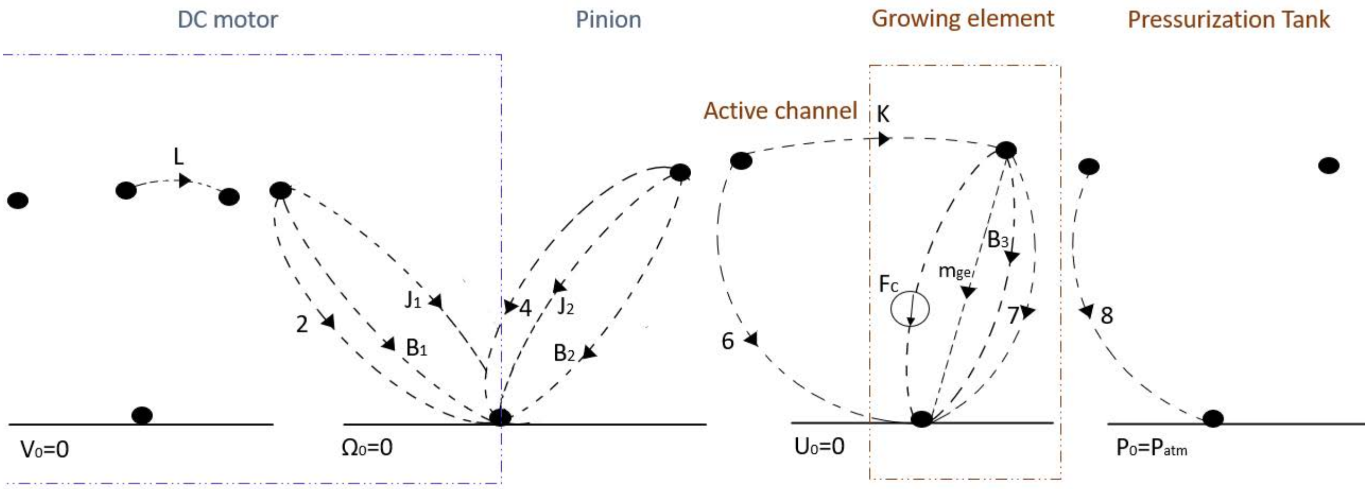

Figure 4.5: Links of eversion system and of complete system.

4.2.3 Variables of the system

The variables and parameters of the system that are going to be used to form the equations of the system are given in the table that follows:

V_s	Voltage source
R	Resistance
L	Inductor
V_1	Voltage of electric subsystem of the DC motor
Ω_2	Rotational motion of the mechanical rotational subsystem of the DC motor
B_1	Coefficient of viscous friction of the two rotational gears of the dc motor
J_1	Inertia of rotational part of the DC motor
Ω_3	angular velocity of the two rotational gears
T_4	Torque of the pinion
J_2	Inertia of the pinion
B_2	Coefficient of viscous friction of the pinion
Ω_5	angular velocity of pinion
U_6	Linear Velocity of the active channel that occurs from the pinion's rotational motion
m_{ac}	Mass of the active channel
K	spring constant
Fc	Coulomb's Friction as a source
m_{ge}	Mass of the growing element
B_3	viscous friction of the growing element
U_7	linear velocity of active channel
P_8	Pressure of pressurization tank tranduced by the gyrator
Rf	constant of Resistance fluid
P_s	Pressure source

Primary Variables: $V_S, V_R, i_L, V_1, T_2, T_{B_1}, T_{J_1}, \Omega_3, T_4, T_{J_2}, T_{B_2}, \Omega_5, F_6, U_{m_{ac}}, F_k, F_{B_3}, F_c,$ $U_{m_{ge}}, F_7, Q_8, P_{Rf}, P_s$

Secondary Variables: $i_S, i_R, V_L, i_1, \Omega_2, \Omega_{B_1}, \Omega_{J_1}, T_3, \Omega_4, \Omega_{J_2}, \Omega_{B_2}, T_5, U_6, F_{m_{ac}}, U_k, U_{B_3}, U_c,$ $F_{m_{ge}}, U_7, P_8, Q_{Rf}, Q_s$

State variables: $i_L, U_{m_{ac}}, F_k, U_{m_{ge}}$

System's Order: 4

Nd : 4

4.2.4 Elemental equations of the complete system

The Elemental equations are: B - S = 22 - 3 = 19

$$
\begin{aligned}
V_R &= i_R \cdot R && (4.4)\\
\frac{di_L}{dt} &= \frac{1}{L} \cdot V_L && (4.5)\\
V_1 &= -Kt \cdot \Omega_2 && (4.6)\\
T_2 &= Kt \cdot i_1 && (4.7)\\
\Omega_3 &= -n \cdot \Omega_4 && (4.8)\\
T_{B_1} &= B_1 \cdot \Omega_{B_1} && (4.9)\\
T_{J_1} &= J_1 \cdot \frac{d\Omega_{J_1}}{dt} && (4.10)\\
T_4 &= n \cdot T_3 && (4.11)\\
T_{J_2} &= J_2 \cdot \frac{d\Omega_{J_2}}{dt} && (4.12)\\
T_{B_2} &= B_2 \cdot \Omega_{B_2} && (4.13)\\
\Omega_5 &= \frac{1}{\rho} \cdot U_6 && (4.14)\\
F_6 &= -\frac{1}{\rho} \cdot T_5 && (4.15)\\
F_{B_3} &= B_3 \cdot \Omega_{B_3} && (4.16)\\
\frac{dU_{m_{ac}}}{dt} &= \frac{1}{m_{ac}} \cdot F_{m_{ac}} && (4.17)\\
\frac{dF_k}{dt} &= k \cdot U_k && (4.18)\\
F_7 &= P_8 \cdot (-A) && (4.19)\\
Q_8 &= \frac{U_7}{A} && (4.20)\\
P_Rf &= Q_Rf \cdot Rf && (4.21)\\
\frac{dU_{m_{ge}}}{dt} &= \frac{1}{m_{ge}} \cdot F_{m_{ge}} && (4.22)
\end{aligned}
$$

4.2.5 Continuity equations of the complete system

Continuity equations: $N - N_d - S_A = 13 - 4 - 2 = 7$

$$i_R = i_L \tag{4.23}$$

$$i_1 = i_L \tag{4.24}$$

$$T_2 + T_{B_1} + T_{J_1} + T_3 = 0 \tag{4.25}$$

$$\begin{aligned} T_4 + T_{B_2} + T_{J_2} + T_5 &= 0 \\ \Rightarrow T_5 &= -T_4 - T_{B_2} - T_{J_2} \end{aligned} \tag{4.26}$$

$$\begin{aligned} F_6 + F_{m_{ac}} + F_k &= 0 \\ \Rightarrow F_{m_{ac}} &= -F_6 - F_k \end{aligned} \tag{4.27}$$

$$\begin{aligned} F_k - F_{B_3} - F_{m_{ge}} - Fc - F_7 &= 0 \\ \Rightarrow F_{m_{ge}} &= F_k - F_{B_3} - Fc - F_7 \end{aligned} \tag{4.28}$$

$$Q_8 = Q_R f \tag{4.29}$$

4.2.6 Compatibility equations of the complete system

Compatibility equations: $B - N + N_d - S_T = 22 - 13 + 4 - 1 = 12$

$$\begin{aligned} V_S &= V_R + V_L + V_1 \\ \Rightarrow V_L &= V_S - V_R - V_1 \end{aligned} \tag{4.30}$$

$$\Omega_2 = \Omega_3 \tag{4.31}$$

$$\Omega_{B_1} = \Omega_3 \tag{4.32}$$

$$\Omega_{J_1} = \Omega_3 \tag{4.33}$$

$$\Omega_4 = \Omega_5 \tag{4.34}$$

$$\Omega_{J_2} = \Omega_5 \tag{4.35}$$

$$\Omega_{B_2} = \Omega_5 \tag{4.36}$$

$$U_6 = U_{m_{ac}} \tag{4.37}$$

$$U_{B_3} = U_{m_{ge}} \tag{4.38}$$

$$U_7 = U_{m_{ge}} \tag{4.39}$$

$$\begin{aligned} U_{m_{ac}} - U_k - U_{m_{ge}} &= 0 \\ \Rightarrow U_k &= U_{m_{ac}} - U_{m_{ge}} \end{aligned} \tag{4.40}$$

$$\begin{aligned} P_8 + P_R f &= P_S \\ \Rightarrow P_8 &= P_S - P_R f \end{aligned} \tag{4.41}$$

4.2.7 Final elemental equations after substitution

The **final elemental equations** are the following:

$$
\begin{aligned}
V_R &= i_R \cdot R && (4.42)\\
\Rightarrow V_R &= i_L \cdot R && (4.43)\\
\frac{di_L}{dt} &= \frac{1}{L} \cdot V_L && (4.44)\\
\Rightarrow \frac{di_L}{dt} &= \frac{1}{L} \cdot (V_S - V_R - V_1) && (4.45)\\
V_1 &= -Kt \cdot \Omega_2 && (4.46)\\
\Rightarrow V_1 &= -Kt \cdot \Omega_3 && (4.47)\\
T_2 &= Kt \cdot i_1 && (4.48)\\
\Rightarrow T_2 &= Kt \cdot i_L && (4.49)\\
\Omega_3 &= -n \cdot \Omega_4 && (4.50)\\
\Rightarrow \Omega_3 &= -n \cdot \Omega_5 && (4.51)\\
\Rightarrow \Omega_5 &= -\frac{\Omega_3}{n} && (4.52)\\
T_{B_1} &= B_1 \cdot \Omega_{B_1} && (4.53)\\
\Rightarrow T_{B_1} &= B_1 \cdot \Omega_3 && (4.54)\\
T_{J_1} &= J_1 \cdot \frac{d\Omega_{J_1}}{dt} && (4.55)\\
\Rightarrow T_{J_1} &= J_1 \cdot \frac{d\Omega_3}{dt} && (4.56)\\
T_4 &= n \cdot T_3 && (4.57)\\
\Rightarrow T_4 &= n \cdot (-T_{J_1} - T_{B_1} - T_2) && (4.58)\\
\Rightarrow T_4 &= -n \cdot (T_{J_1} + T_{B_1} + T_2) && (4.59)\\
T_{J_2} &= J_2 \cdot \frac{d\Omega_{J_2}}{dt} && (4.60)\\
\Rightarrow T_{J_2} &= J_2 \cdot \frac{d\Omega_5}{dt} && (4.61)\\
T_{B_2} &= B_2 \cdot \Omega_{B_2} && (4.62)\\
\Rightarrow T_{B_2} &= B_2 \cdot \Omega_5 && (4.63)\\
\Omega_5 &= \frac{1}{\rho} \cdot U_6 && (4.64)\\
\Rightarrow \Omega_5 &= \frac{1}{\rho} \cdot U_{m_{ac}} && (4.65)\\
& && (4.66)
\end{aligned}
$$

$$\begin{aligned}
F_6 &= -\frac{1}{\rho}\cdot(-T_4 - T_{B_2} - T_{J_2}) && (4.67)\\
\Rightarrow F_6 &= \frac{1}{\rho}\cdot(T_4 + T_{B_2} + T_{J_2}) && (4.68)\\
F_{B_3} &= B_3\cdot\Omega_{B_3} && (4.69)\\
\Rightarrow F_{B_3} &= B_3\cdot U_{m_{ge}} && (4.70)\\
\frac{dU_{m_{ac}}}{dt} &= \frac{1}{m_{ac}}\cdot F_{m_{ac}} && (4.71)\\
\Rightarrow \frac{dU_{m_{ac}}}{dt} &= \frac{1}{m_{ac}}\cdot(-F_6 - F_k) && (4.72)\\
\frac{dF_k}{dt} &= k\cdot U_k && (4.73)\\
\Rightarrow \frac{dF_k}{dt} &= k\cdot\left(U_{m_{ac}} - U_{m_{ge}}\right) && (4.74)\\
F_7 &= P_8\cdot(A-) && (4.75)\\
\Rightarrow F_7 &= (P_Rf - P_s)\cdot A && (4.76)\\
Q_8 &= \frac{U_7}{A} && (4.77)\\
\Rightarrow Q_8 &= \frac{U_{m_{ge}}}{A} && (4.78)\\
P_Rf &= Q_Rf\cdot Rf && (4.79)\\
\Rightarrow P_Rf &= Q_8\cdot Rf && (4.80)\\
\frac{dU_{m_{ge}}}{dt} &= \frac{1}{m_{ge}}\cdot F_{m_{ge}} && (4.81)\\
\Rightarrow \frac{dU_{m_{ge}}}{dt} &= \frac{1}{m_{ge}}\cdot(F_k - F_{B_3} + F_C - F_7) && (4.82)
\end{aligned}$$

The resulting equations that retrieved from above and are going to be used later for the formulation of the state equations are:

$$\Omega_3 = -n\cdot\Omega_5 \Rightarrow \Omega_3 = -n\cdot\frac{1}{\rho}\cdot U_{m_{ac}} \qquad (4.83)$$

$$P_Rf = Q_8\cdot Rf = \frac{U_{m_{ge}}\cdot Rf}{A} \Rightarrow P_Rf = \frac{U_{m_{ge}}\cdot Rf}{A} \qquad (4.84)$$

$$V_1 = -Kt\cdot\Omega_3 = -Kt\cdot(-n\cdot\Omega_5) = Kt\cdot n\cdot\Omega_5 = Kt\cdot n\cdot\frac{1}{\rho}\cdot U_{m_{ac}} \qquad (4.85)$$

4.2.8 State equations of the complete system

The system's state equations are the following and describe how the system's state variables change over time based on the system's inputs and internal dynamics and are expressed in terms of a set of state variables:

$$\frac{di_L}{dt} = \frac{1}{L}\left(V_S - V_R - V_1\right) \tag{4.86}$$

From (4.85)

$$\frac{di_L}{dt} = \frac{1}{L}\left(V_S - R \cdot i_L - Kt \cdot n \cdot \frac{1}{\rho} \cdot U_{m_{ac}}\right) \tag{4.87}$$

The state equation that describes the rate of change of the velocity of the active channel according to time is (based on F_6 equation 3.74 of the previous chapter):

$$\begin{aligned}
\frac{dU_{m_{ac}}}{dt} &= \frac{1}{m_{ac}}\left(-F_6 - F_k\right) \Rightarrow \\
\frac{dU_{m_{ac}}}{dt} &= \frac{1}{m_{ac}}\left(\frac{n \cdot Kt \cdot i_L}{\rho} - U_{m_{ac}} \cdot \left(B_1 \cdot n^2 \cdot \frac{1}{\rho^2} + B_2 \cdot \frac{1}{\rho^2}\right)\right. \\
&\qquad \left. - \frac{dU_{m_{ac}}}{dt}\left(J_1 \cdot n^2 \cdot \frac{1}{\rho^2} + J_2 \cdot \frac{1}{\rho^2}\right) - F_k\right) \Rightarrow \\
\frac{dU_{m_{ac}}}{dt}\,(1 + J_1 \cdot n^2 \cdot \frac{1}{\rho^2 \cdot m_{ac}} &+ J_2 \cdot \frac{1}{\rho^2 \cdot m_{ac}}\;) = \frac{n \cdot Kt \cdot i_L}{\rho \cdot m_{ac}} \\
&\qquad - U_{m_{ac}} \cdot \left(B_1 \cdot n^2 \cdot \frac{1}{\rho^2 \cdot m_{ac}} + B_2 \cdot \frac{1}{\rho^2 \cdot m_{ac}}\right) - \frac{F_k}{m_{ac}} \Rightarrow \\
\frac{dU_{m_{ac}}}{dt} &= \frac{\frac{\rho \cdot n \cdot Kt \cdot i_L - U_{m_{ac}}(B_1 \cdot n^2 + B_2) - F_k \cdot \rho^2}{\rho^2 \cdot m_{ac}}}{\frac{\rho^2 \cdot m_{ac} + J_1 \cdot n^2 + J_2}{\rho^2 \cdot m_{ac}}} \Rightarrow \\
\frac{dU_{m_{ac}}}{dt} &= \frac{\rho \cdot n \cdot Kt \cdot i_L - U_{m_{ac}}(B_1 \cdot n^2 + B_2) - F_k \cdot \rho^2}{\rho^2 \cdot m_{ac} + J_1 \cdot n^2 + J_2}
\end{aligned} \tag{4.88}$$

The state equation that describes the rate of change of the velocity of the growing element according to time is:

$$\begin{aligned}
\frac{dU_{m_{ge}}}{dt} &= \frac{1}{m_{ge}} \cdot F_{m_{ge}} \\
&= \frac{1}{m_{ge}}(F_k - F_{B_3} - F_c - F_7) \\
&= \frac{1}{m_{ge}}\left(F_K - B_3 \cdot U_{m_{ge}} - F_c - (P_R f - P_s)\right) \\
&= \frac{1}{m_{ge}}\left(F_k - B_3 \cdot U_{m_{ge}} - F_c + P_s \cdot A - P_R f \cdot A\right) \\
&= \frac{1}{m_{ge}}\left(F_k - U_{m_{ge}}\,(B_3 + 1) - F_c + P_s \cdot A\right) \\
\Rightarrow \frac{dU_{m_{ge}}}{dt} &= \frac{1}{m_{ge}}\left(F_k - U_{m_{ge}}\,(B_3 + 1) - F_c + P_s \cdot A\right)
\end{aligned} \tag{4.89}$$

The state equation that describes the rate of change of spring's force according to time is:

$$
\begin{aligned}
\frac{dF_k}{dt} &= k \cdot U_k \\
\Rightarrow \frac{dF_k}{dt} &= k \cdot \left(U_{m_{ac}} - U_{m_{ge}}\right)
\end{aligned}
\tag{4.90}
$$

4.2.9 Matrix Formulation

The complete system model for a linear time-invariant system consists of a set of n state equations, defined in terms of the matrices A and B, and a set of output equations that relate any output variables of interest to the state variables and inputs, and expressed in terms of the **C** and **D** matrices [15]:

$$\mathbf{y} = \mathbf{C}\mathbf{x} + \mathbf{D}\mathbf{u} \tag{4.91}$$

The **y** variable each time depends on the elements that is needed to be measured as output. The state equations in terms of the elements should be written in a matrix in the form of

$$\dot{\mathbf{x}} = \mathbf{A}\mathbf{x} + \mathbf{B}\mathbf{u} \tag{4.92}$$

In this specific case, due to the presence of multiple sources, the equation is formulated as follows:

$$\dot{\mathbf{x}} = \mathbf{A}\mathbf{x} + \mathbf{B_1}\mathbf{u_1} + \mathbf{B_2}\mathbf{u_2} \tag{4.93}$$

where: **x** is the state-vector and is given by

$$\mathbf{x} = \begin{bmatrix} i_L \\ F_k \\ U_{m_{ac}} \\ U_{m_{ge}} \end{bmatrix} \tag{4.94}$$

A is the system matrix given by

$$\mathbf{A} = \begin{bmatrix} -\frac{R}{L} & 0 & -\frac{Kt \cdot n}{\rho \cdot L} & 0 \\ 0 & 0 & K & -K \\ \frac{\rho \cdot n \cdot Kt}{m_{ac} \cdot \rho^2 + J_1 \cdot n^2 + J_2} & -\frac{1}{\rho^2} & -B_1 \cdot n^2 + B_2 & 0 \\ 0 & \frac{1}{m_{ge}} & 0 & \frac{-B_3 - 1}{m_{ge}} \end{bmatrix} \tag{4.95}$$

The input matrix $\mathbf{B_1}$ is given by

$$\mathbf{B_1} = \begin{bmatrix} \frac{1}{L} \\ 0 \\ 0 \\ 0 \end{bmatrix} \tag{4.96}$$

and relates the system inputs to the state variables $\mathbf{x}$. Vector $\mathbf{u}$ represents the input vector, which is in this case is a scalar given by the voltage source V_S

$$\mathbf{u} = V_s \tag{4.97}$$

The input matrix $\mathbf{B_2}$ is given by

$$\mathbf{B_2} = \begin{bmatrix} 0 \\ 0 \\ 0 \\ \frac{1}{m_{ge}} \end{bmatrix} \tag{4.98}$$

The sources that are applied to the system and represent the vector in this case are:

$$\mathbf{u} = -F_c + P_s \cdot A \tag{4.99}$$

Specifically, the matrices are formed like this:

$$\frac{d}{dt}\begin{bmatrix} i_L \\ F_k \\ U_{m_{ac}} \\ U_{m_{ge}} \end{bmatrix} = \begin{bmatrix} -\frac{R}{L} & 0 & -\frac{Kt \cdot n}{\rho \cdot L} & 0 \\ 0 & 0 & K & -K \\ \frac{\rho \cdot n \cdot Kt}{m_{ac} \cdot \rho^2 + J_1 \cdot n^2 + J_2} & -\frac{1}{\rho^2} & -B_1 \cdot n^2 + B_2 & 0 \\ 0 & \frac{1}{m_{ge}} & 0 & \frac{-B_3 - 1}{m_{ge}} \end{bmatrix} \cdot \begin{bmatrix} i_L \\ F_k \\ U_{m_{ac}} \\ U_{m_{ge}} \end{bmatrix} + \begin{bmatrix} \frac{1}{L} \\ 0 \\ 0 \\ 0 \end{bmatrix} \cdot V_s + \begin{bmatrix} 0 \\ 0 \\ 0 \\ \frac{1}{m_{ge}} \end{bmatrix} - F_c + P_s \cdot A \tag{4.100}$$

4.3 Forces and Frictions

In order to simulate the system's behavior, the frictions and forces applied to the system must be studied analytically. A simple representation of the physical analysis is shown in the figure 4.6 below:

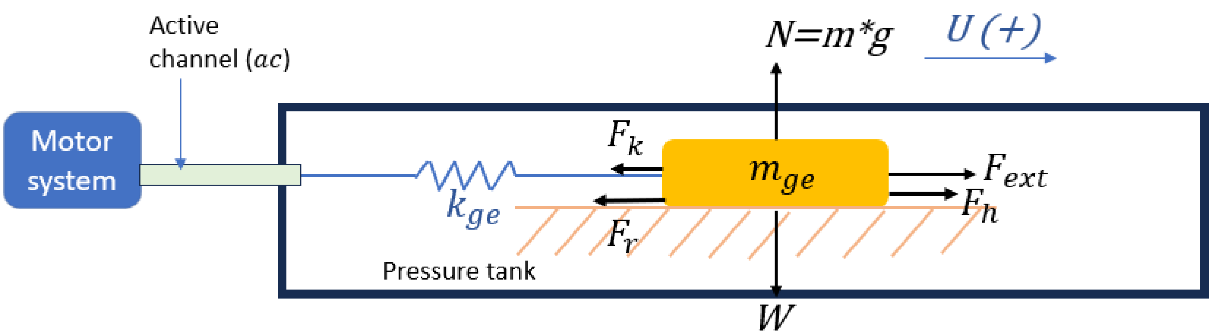

Figure 4.6: Forces that are applied to the system.

Where

- F_k: Spring's Force that tends to return it to its natural length.
- F_h: Hydraulic Force due to the pressure that exists inside the tank $F_h = P_s \cdot A$.
- F_{ext}: External Force applied to the system because of the growing element.
- N: Vertical Force of the ground applied to the growing element.
- W: Weight of the growing element.
- F_r: Coulomb's Friction (F_c).

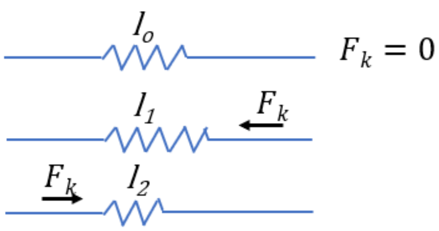

Figure 4.7: Spring's Force according to its displacement.

The frictions applied to the system include the viscous friction due to the fluid environment and static friction, which transitions to sliding friction once it exceeds its limit. When the equilibrium conditions are applied, there is no friction, and the relation connecting the forces acting on the growing element is given by (based on fig. 4.6):

$$\Sigma F = 0 \Rightarrow F_{ext} - F_k - F_r + F_h = 0 \Rightarrow F_{ext} = F_k - F_h + F_r \tag{4.101}$$

When the object starts moving, with the right direction considered positive, sliding friction F_s is applied. Friction value depends on whether the condition is static or sliding. If it is static then the value of static friction depends on the sum of the rest of the forces applied on the body. This system is non-linear due to the frictions that are applied. The algebraic expression describing the applied static friction is:

$$Fr_{static} = F_{ext} - F_k + F_h \tag{4.102}$$

When the equilibrium conditions no longer apply, Newton's second law begins to take effect:

$$\Sigma F = m \cdot a \tag{4.103}$$

The static friction (F_s) is applied to the system, and when it exceeds its limit

$$F_c < \mu \cdot N \tag{4.104}$$

sliding friction begins to occur. When $F_{ext} > F_c$, the growing element starts its movement. In this condition, the algebraic expression of the friction is:

$$Friction = -F_c \cdot \mathrm{sign}(F_{ext} - F_s) \tag{4.105}$$

These expressions are explained in detail in the following friction's diagram. The Stribeck friction is the negatively sloped characteristic taking place at low velocities. The Coulomb friction, F_c, results in a constant force at any velocity. The viscous friction, F_v, opposes motion with the force directly proportional to the relative velocity. The sum of the Coulomb and Stribeck frictions at the vicinity of zero velocity is often referred to as the breakaway friction, F_{brk} (see Figure 4.8).

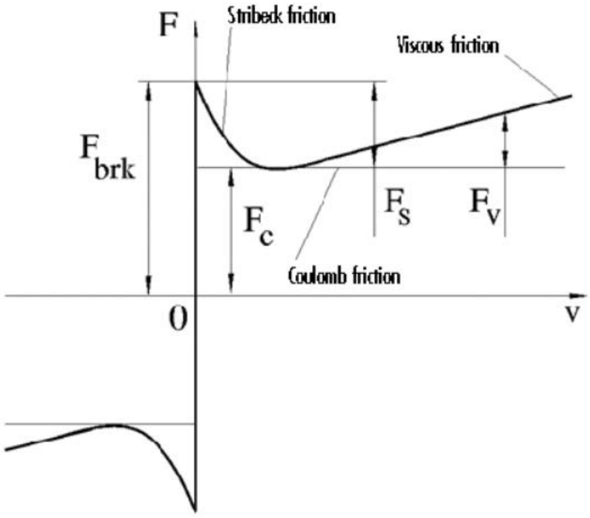

Figure 4.8: Translational Friction block [21].

4.4 Simulation results

The MATLAB code simulates the behavior of this whole system over time and plots the current, the linear velocities of the active channel and of the growing element and the spring's force. ODE45 function can integrate both linear and non-linear systems, but it cannot integrate discontinuous systems (cannot guarantee convergence). Due to the frictions that are applied to the system, this whole system is discontinuous. In order to be able for the ODE to integrate these state equations, the frictions have to be divided into sub conditions, so that this function won't come up with any discontinuity. The variable DU_m in the following code represents an area where the velocity is almost zero, but Matlab cannot recognize these areas and creates instability to the system. That's why Friction has to be calculated in each condition.

```
%file_name: whole_system.m
    clear;
    close all;
    y0 = [0 0 0 0];          %[current; spring;  velocity_ac;
       velocity_ge;]
    tspan = [0 5];       %5 seconds

    % parameters of the ODE45
    parameters_integration;

    options = odeset('RelTol', reltol, 'AbsTol', abstol,...
                'MaxStep', maxstep, 'InitialStep', initstep);


    [t, y] = ode45(@(t,y)DCpneumaticSystem(t,y), tspan, y0, options);

    % Plot
    figure;
    subplot(4,1,1);
    plot(t, y(:, 1));
    xlabel('Time [sec]');
    ylabel('Current iL [A]');
    title('DC Hydraulic System - Current');

    subplot(4,1,2);
    plot(t, y(:, 2));
    xlabel('Time [sec]');
    ylabel('Spring Force [N] ');
    title('Hydraulic System - Spring Force ');

    subplot(4,1,3);
    plot(t, y(:, 3));
    xlabel('Time [sec]');
    ylabel('Linear Velocity [m/sec] ');
    title('DC Hydraulic System - Linear Velocity ac');


    subplot(4,1,4);
    plot(t, y(:, 4));
    xlabel('Time [sec]');
    ylabel('Linear Velocity [m/sec] ');
    title('Hydraulic System - Linear Velocity ge ');

    function dydt = DCpneumaticSystem(t, y)
```

```
parameters;
dydt = zeros(4,1);
y1=y(1); %iL - current
y2=y(2); %Fk - spring force
y3=y(3); %Um_ac - linear velocity ac
y4=y(4); %Um_ge - linear velocity ge

ForceE = Ps*A + y2; %calculate force external

% Calculate frictional force Fr based on the sign of y4 -> Um_ge
if ((y4 < DUm) && (y4 > -DUm))  %DUm is almost zero
    y4 = 0;
    if (ForceE < fr_static)
        Fr = ForceE; %equilibrium condition
    else Fr = fr_static*sign(ForceE); %with or without (-) at the
       start
    end
else Fr = -Fc * sign(ForceE-fr_static);

end

%diL/dt:
dydt1 = (Us-(R*y1)-Kt*n*(1/rd)*y3)/L;

%dFk/dt:5
dydt2=-K*(y4-y3); %Fk=-k*Dx

%dUm_ac/dt:
dydt3 =(rd*n*Kt*y1 - y3*(B1*(n^2)+B2) - y2*(rd^2))/m_ac*(rd^2+J1*(
   n^2)+J2);

%dUm_ge/dt:
dydt4 =(y2 - y4*(B3+1) - Fr + Ps*A)/m_ge;


dydt=[dydt1; dydt2; dydt3; dydt4];
end
```

The parameter's files that were included were the following:

```
%file_name: parameters.m
    % Define the parameters
    A =  5*pi*(0.003)^2; %m^2
    Us = 5; %volt
    Rf =  259352.704259; % kg/(m^4 s)
    Ps = 150000; %Pascal, 150kPa
    K = 10^3; %stable coefficient of the spring;
```

```
    %m = 5*10^(-4); %kg, the mass of the growing element and the added
        mass of displaced
    % fluid
    Fc = 11.999; %coulomb friction
    fr_static = 12.999; %static friction

    DUm=10^(-6); %m/sec

    n=1/200;
    J2=0.0078; %g*m^2, moment of inerta of pinion
    R=0.198;
    L=0.128*10^(-3);
    Kt=1.5;
    rd=2*10^(-3); %m radius of the pinion
    tconstant=1.16*10^(-3); %S
    B2=0.1; %viscous friction of pinion
    B1=0.05; %viscous friction of dc motor
    B3=(320*10^(-3)/((8130*2*pi)/60)); %viscous friction of ge+rack+ac
    J1=0.0058; %g*m^2  , moment of inertia of dc motor

    m_ge=10^(-4);
    m_ac=4*10^(-4);
```

```
%file_name: parameters_integration
    % parameters of the ODE45

    reltol = 1e-3;
    abstol = [1e-5 1e-5 1e-5 1e-5];
    maxstep = 1e-2;
    initstep = 0.001;
```

The simulation results that arose from the integration are illustrated in the following figures. In the first graphic representation, where the current is studied, the current has very high values, but it reaches a steady state almost immediately, which is a little bit more than 20 [A]. Also, it develops its constant value almost immediately. In the second graphic representation, the behavior of the spring's force is simulated. At the beginning (t=0), the spring force starts with a high value, both positive and negative. This indicates an initial transient response likely due to the system starting from the rest (equilibrium conditions). There is an oscillation because the growing element starts its movement, so the length of the spring is adapting to the desirable condition of the motion. As time progresses, these oscillations decay rapidly, indicating a significant damping effect in the system. The damping force is likely dissipating the energy, reducing the amplitude of the oscillations over time. Eventually, the system reaches a steady state with a spring force of -10N, indicating that the active channel is also moving and causing the spring to stretch. This occurs because the growing element is in motion, but the active channel restricts it from moving at a higher velocity. Essentially, the active channel is holding the element back, which stretches the spring. The spring force tends to restore the spring to its original length, assuming the direction of force is to the left. The velocities of the active channel and of the growing element reach the value of $5 \cdot 10^{-3}$ m/sec. In the diagram of the active channel's velocity, the initial value is zero and it starts increasing gradually. In the figures 4.9 and 4.11, the results show that the growing element and the active channel have developed almost the same value of the velocity at the same time, which indicates that the simulation is correct and successful.

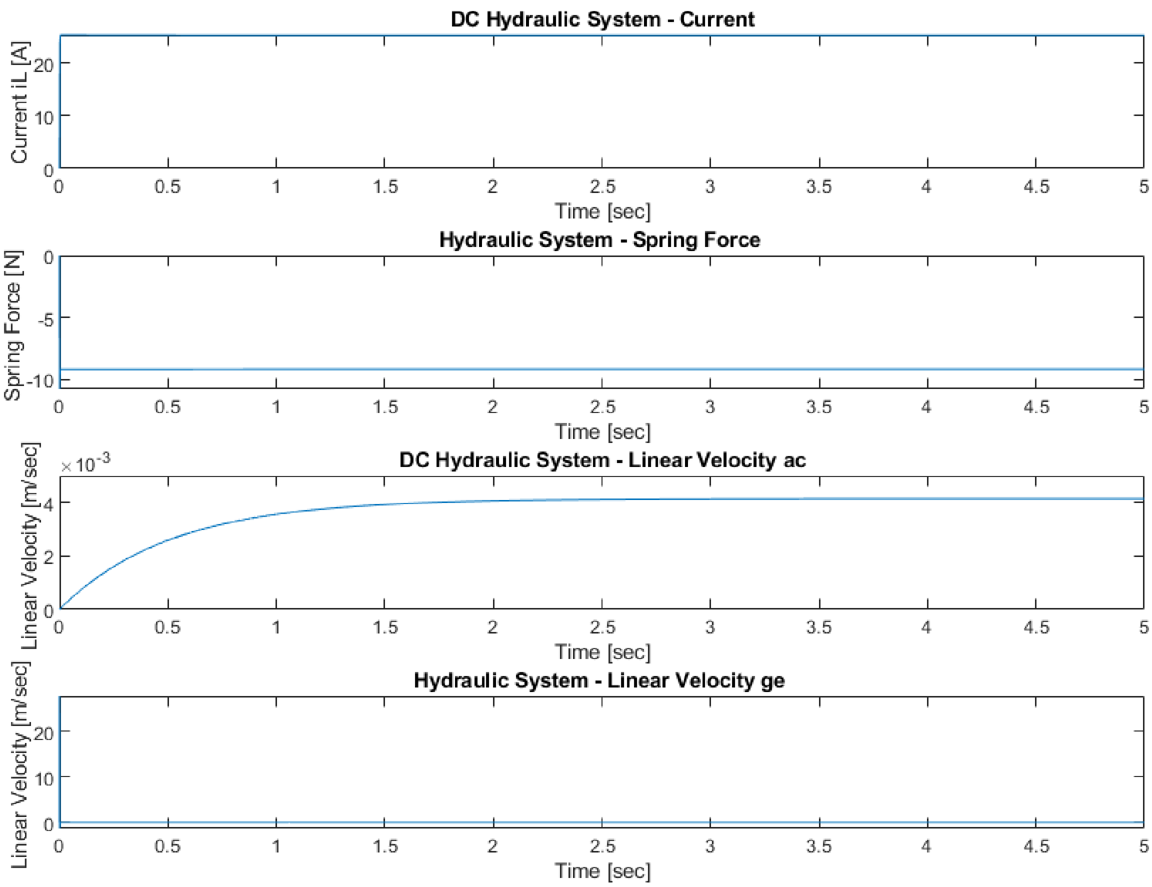

Figure 4.9: Figures of current, spring's force, active channel's velocity and growing element's velocity.

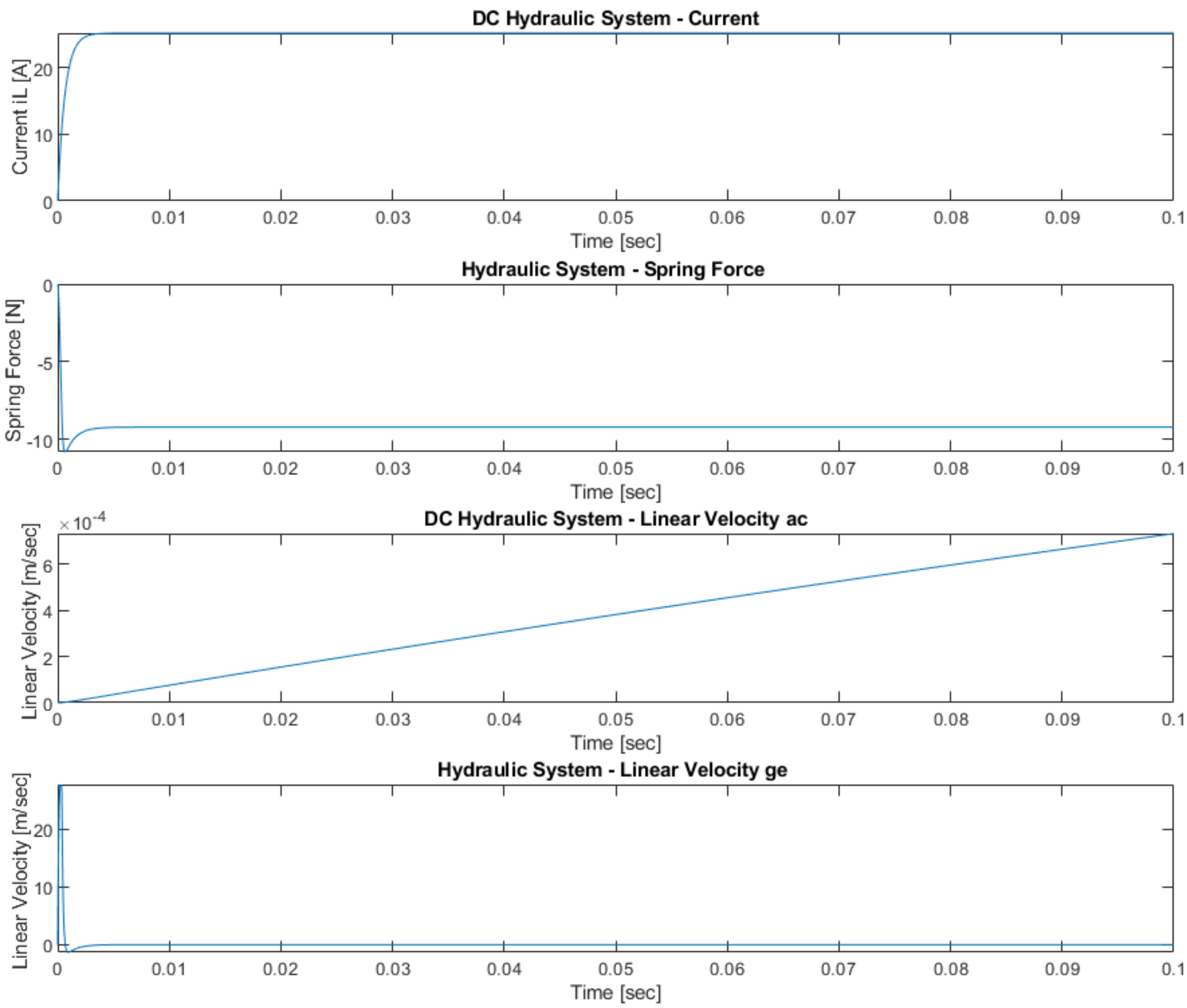

Figure 4.10: Figures of current, spring's force, active channel's velocity and growing element's velocity for 0.1 sec, where oscillations are shown because of the transient response.

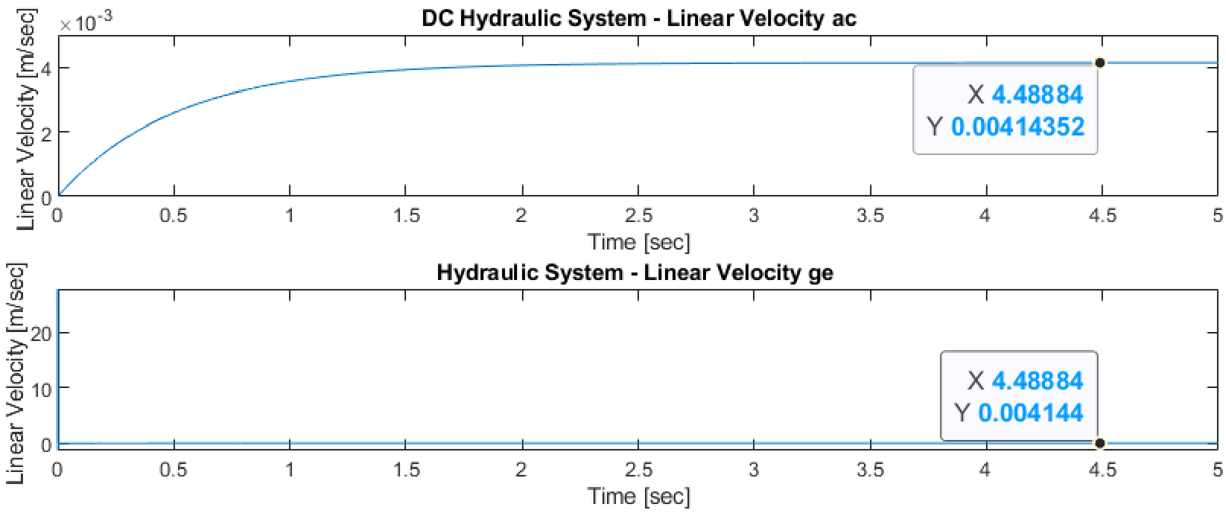

Figure 4.11: Figures of Velocities for the Active Channel and the Growing Element.

4.5 Conclusions

In this chapter, the complete system was examined and analysed. This includes the DC motor, the pinion, the active channel, the growing element and the pressurization tank. The process that was followed was the same as in the previous chapter. Modeling techniques were employed to develop linear graphs, normal trees, and links. The variables describing the system's dynamics were classified, resulting in the formation of equations for elements, continuity, stability, and state. The state equations, which describe the system's behavior at specific times, were derived from these foundational equations. Following this, matrices that describe the system's output were also constructed, providing a comprehensive representation of the system's dynamics. Furthermore, the Two-Port Energy Transducing Elements were studied, specifically Gyrators, that transduce mechanical energy to hydraulic and the opposite. These elements involve variables known as power variables, as their multiplication yields the system's power. Moreover, the frictions that are applied in the growing element were studied, as the Coulomb's friction causes discontinuity to the system, which causes problems in the integration.

Afterward, the state equations were implemented in Matlab to simulate and integrate the system. Through this integration, the state variables could be examined when plotted. The plot that represents the current's value over time, exhibits very high values during the transient response, quickly stabilizing to a steady state slightly above 20 A. in the second plot, which represents the behavior of spring force, which its initial values are negative or positive, indicative of an initial transient response likely due to the system starting from equilibrium 4.10. As the growing element initiates movement, the spring length adjusts to achieve desired motion conditions, resulting in oscillations that decay rapidly. This decay signifies significant damping within the system, dissipating energy and reducing oscillation amplitudes over time. Ultimately, the system reaches a steady state indicating equilibrium as the active channel moves and stretches the spring. In the third and fourth plot, the velocities of both the active channel and the growing element converge to a very good value and they move with the same velocity. This synchronization indicates that the simulation was successful, as the active channel moves together with the growing element.

Chapter 5

Automatic Control System

A system comprises elements contained within a boundary, interconnected in a manner that enables them to interact and perform specific tasks. Control refers to the process of directing a system to operate in a desired manner. An automatic control system consists of interconnected components designed to guide a controlled system towards a predefined response, without human intervention. These systems are categorized as either natural or artificial [13]. Until now, the simulation's control was open loop, but now it will become closed loop, i.e. the input command will depend on the current output. The voltage source V_s will be controlled with an input signal that depends on the output in order to achieve a desirable output value. The output velocity will be also controlled and based on the desirable value, the voltage source will be adapt to it. In this chapter, the aim of the simulation is the system to has constantly the desirable velocity, which will be defined by the user's needs.
For the system's needs, there will be applied a proportional controller. Proportional control is a control system technology in which the response (output) is proportional to the difference between a setpoint value (desired) and the current value of a process variable. The error should be minimized as the process is coming to the desirable setpoint.

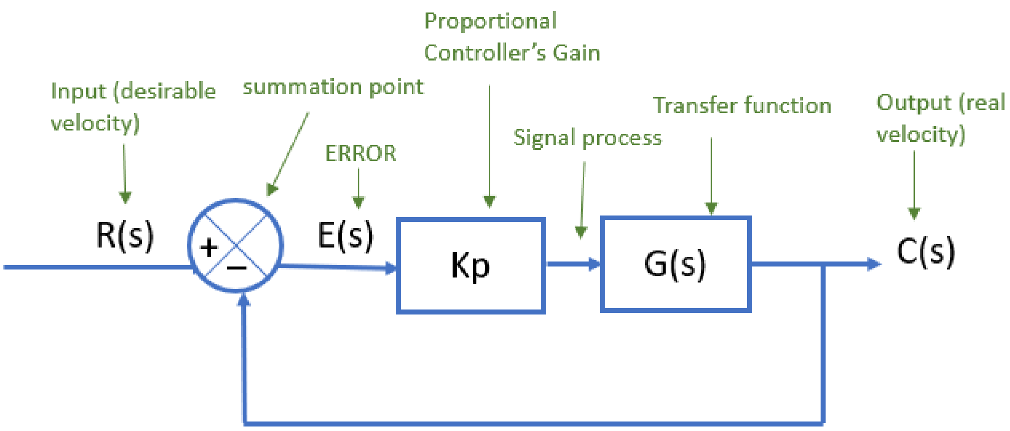

Figure 5.1: Block diagram of proportional control.

The error is calculated as:

$$E(t) = C(t) - R(t) \quad (time\ domain) \tag{5.1}$$

When considering Laplace transforms:

$$E(s) = C(s) - R(s) \quad (frequency\ domain) \tag{5.2}$$

where:

- $C(s)$ represents the actual output.
- $R(s)$ represents the reference or desired output.

In closed-loop control systems, the objective is to minimize this error $E(s)$ to achieve the desired output $R(s)$. This process ensures that the system responds effectively to deviations from the desired state, maintaining stability and accuracy in its operation. The signal process is the control signal or action that will be applied to the system based on the error. In proportional control is calculated as:

$$Signal\ process = E(s) \cdot K_p \tag{5.3}$$

where:

- $E(s)$ is the difference between the desired setpoint (reference) and the actual output of the system. It represents how far the system's current state deviates from the desired state
- K_p is the proportional gain, a constant parameter that scales the error signal to generate the control signal. It determines the strength of the control action relative to the error.

Chapter 6

Control of the complete system

Inside the DC pneumatic System function (DCpneumaticSystem), the error is calculated and control signal is determined for the proportional control action for each time step of the simulation. The error variable represents the difference between the desired velocity of the growing element and the actual velocity. Then, with this error the control signal is calculated based on the proportional gain Kp. After the ODE solver (ode45) is called and the simulation results are obtained, the error and the control signal are calculated again. This allows the plot of error over time and visualize how the proportional control action affects the system's performance throughout the simulation. In summary all these variables are calculated both inside and outside the function for different purposes: inside for determining the control action during each time step of the simulation, and outside for post-processing and visualization of the simulation results.

```
%file name: active_channel_proportional_control.m
    clear;
    close all;
    y0 = [0 0 0 0];         %[current; spring;  velocity_ac;
       velocity_ge; at initial state]
    tspan = [0 1];
    Kp1=5000000; %defined proportional gain
    y4_des = 3*10^(-3); %defined desired velocity of ac - y3 and y4 -
       ge

    % parameters of the ODE45
    parameters_integration;


    options = odeset('RelTol', reltol, 'AbsTol', abstol,...
                'MaxStep', maxstep, 'InitialStep', initstep);


    [t, y] = ode45(@(t,y)DCpneumaticSystem(t,y,Kp1,y4_des), tspan, y0,
        options);

    % Plot
    figure;
```

```
subplot(4,1,1);
plot(t, y(:, 1));
xlabel('Time [sec]');
ylabel('Current iL [A]');
title('DC Hydraulic System - Current');

subplot(4,1,2);
plot(t, y(:, 2));
xlabel('Time [sec]');
ylabel('Spring Force [N] ');
title('Hydraulic System - Spring Force ');

subplot(4,1,3);
plot(t, y(:, 3));
xlabel('Time [sec]');
ylabel('Linear Velocity [m/sec] ');
title('DC Hydraulic System - Linear Velocity ac');

subplot(4,1,4);
plot(t, y(:, 4));
xlabel('Time [sec]');
ylabel('Linear Velocity [m/sec] ');
title('Hydraulic System - Linear Velocity ge ');

%define error1 of ac and control_signal
error1 = y4_des - y(:,3);
control_signal1 = Kp1 * error1; % Proportional control action

% Plot error
figure;
subplot(3,1,1);
plot(t, error1);
xlabel('Time [sec]');
ylabel('Error in ac Velocity');
title('Proportional Control of Linear Velocity ac');

%plot: control signal1
subplot(3,1,2);
plot(t, control_signal1);
xlabel('Time [sec]');
ylabel('Control Signal of ac');
title('Control signal');


%define error2 of ge
error2 = y4_des - y(:,4);
```

```
% Plot error2
subplot(3,1,3);
plot(t, error2);
xlabel('Time [sec]');
ylabel('Error in ge velocity');
title('Error of Linear Velocity of ge');


function [dydt] = DCpneumaticSystem(t, y,Kp1, y4_des)
parameters;

dydt = zeros(4,1);
y1=y(1); %iL - current
y2=y(2); %Fk - spring force
y3=y(3); %Um_ac - linear velocity ac
y4=y(4); %Um_ge - linear velocity ge - y4_act


% Calculate error and proportional control signal of ac
error1 = y4_des - y3; %ac control velocity
control_signal1 = Kp1 * error1; % Proportional control action

%Calculate error and proportional control signal of ge
error2 = y4_des - y4; %ac control velocity
ForceE = Ps*A + y2; %calculate force external

% Calculate frictional force Fr based on the sign of y4 -> Um_ge
if ((y4 < DUm) && (y4 > -DUm))
    y4 = 0;
    if (ForceE < fr_static)
        Fr = ForceE; %Î£F=0;
    else Fr = fr_static*sign(ForceE); %with or without (-) at the
       start
    end
else Fr = -Fc * sign(ForceE-fr_static);

end

%diL/dt:
dydt1 = (control_signal1-(R*y1)-Kt*n*(1/rd)*y3)/L;

%dFk/dt:
dydt2=-K*(y4-y3); %Fk=-k*DX, (k)'dk = -K*(Delta_x)' dx
%for extended spring y4 >= y3
```

```
    %dUm_ac/dt:
    dydt3 =(rd*n*Kt*y1 - y3*(B1*(n^2)+B2) - y2*(rd^2))/m_ac*rd^2*(J1*(
       n^2)+J2);

    %dUm_ge/dt:
    dydt4 =((y2 - y4*(B3+1) - Fr + Ps*A)/(m_ge)); %actual velocity

    dydt=[dydt1; dydt2; dydt3; dydt4];


     % disp(['Final Error1:' num2str(error1)]);
     % disp(['Final Error2:' num2str(error2)]);


    end
```

The files of the parameters:

```
%file name: parameters_integration.m
% parameters of the ODE45
    reltol = 1e-3;
    abstol = [1e-5 1e-5 1e-5 1e-5];
    maxstep = 1e-2;
    initstep = 0.001;
```

```
%file name: parameters.m
    % Define the parameters
    A =  5*pi*(0.003)^2; %m^2
    Vs = 5; %volt
    Rf =  259352.704259; % kg/(m^4 s)
    Ps = 150000; %Pascal, 150kPa
    K = 10^3; %stable coefficient of the spring;
    %m = 5*10^(-4); %kg, the mass of the growing element and the added
        mass of displaced
    % fluid
    Fc = 11.999; %coulomb friction
    fr_static = 12.999; %static friction

    DUm=10^(-6); %m/sec

    n=50;
    J2=0.0078; %g*m^2, moment of inerta of pinion
    R=0.198;
    L=0.128*10^(-3);
    Kt=1.5;
    rd=2*10^(-3); %m radiant of the pinion
    tconstant=1.16*10^(-3); %S
```

```
B2=0.1; %viscous friction of pinion
B1=0.05; %random value, viscous friction of dc motor
B3=(320*10^(-3)/((8130*2*pi)/60)); %viscous friction of ge+rack+ac
J1=0.0058; %g*m^2  , moment of inertia of dc motor
m_ge=10^(-4);
m_ac=4*10^(-4);
```

Figure 6.1 presents the errors in the velocities of the growing element and of the active channel for a duration of 1 second. The first plot shows the error in ac velocity over time. The error seems to decrease almost immediately, reaching the value of $2.2425 \cdot 10^{-5}$, which is close to zero, indicating the proportional control is reducing the error effectively. The control signal's plot shows the control signal applied to the system as a voltage source. This suggests that the proportional controller is applying a strong correction initially to bring the velocity error down quickly, corresponding to the error reduction. The third plot shows the error in ge velocity over time. The error appears to be approximtely $2.243 \cdot 10^{-5}$, which is very close to zero, indicating that the ge velocity is probably the desired one.

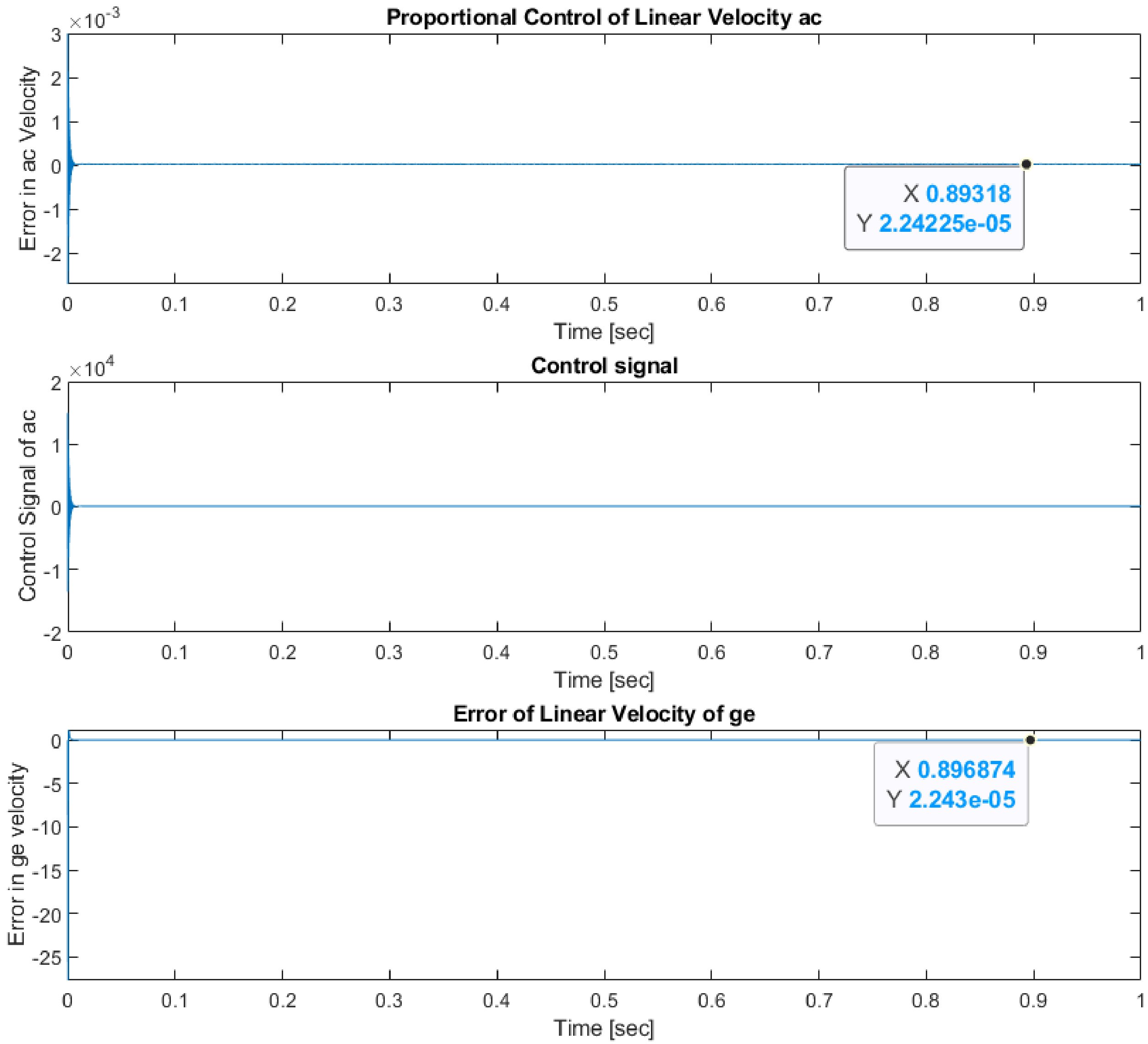

Figure 6.1: Errors and control signal.

The current's plot indicates that the current at the start reaches very high values, but it decreases and reaches a normal value at 2.4 A. When the system starts, the initial error between the desired velocity and the actual velocity is likely quite large. The proportional controller responds to this large initial error by generating a large control signal to quickly reduce the error. This is possible by a high current value being supplied to the motor, so a high current implies a high torque. This high torque is necessary to quickly bring the system to the desired state, overcoming any initial inertia or resistance. The spring force remains negative, suggesting that the active channel holds back the growing element, and that's why the spring is stretched. More specifically, the growing element probably moves a little bit faster than the active channel, so that the spring is constantly stretched, in order to have both of them the same velocity value. The linear velocity of growing element remains almost constant, with a very slight increase. Comparing the two velocities, they have almost the same values at specific times, almost reaching the desired defined values at 3 mm/sec. This probably happens because maybe some values of the parameters are wrong, or the system might need one more control signal for the pressure.

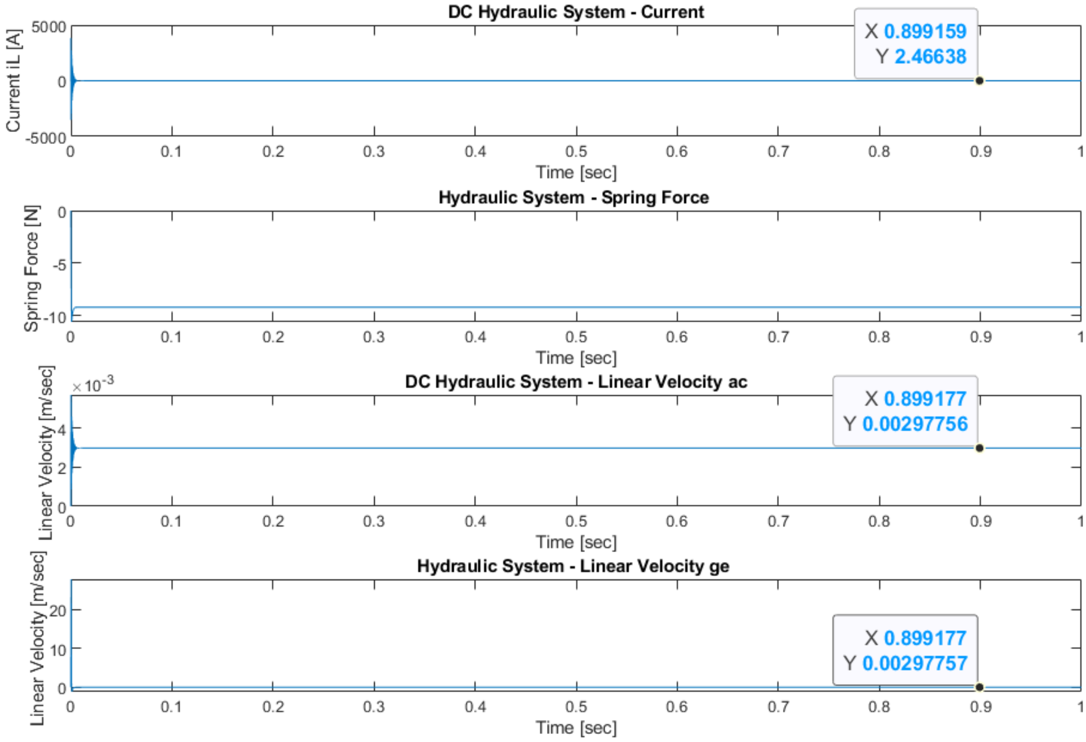

Figure 6.2: Graphic representation of current, spring's force and of velocities of active channel and growing element.

Chapter 7

Conclusions

This thesis focuses on modeling and controlling an eversion growing robot designed for early breast cancer diagnosis. The first chapter discusses the motivation and significance of this research. With cancer statistics reaching alarming levels, early detection holds the potential to save millions of lives. Eversion growing robots, particularly Mammobots, could potentially offer a solution to this problem. Initially employed in archaeology and rescue operations, these robots have diversified into various branches including agriculture, industry, nuclear applications, and now, significantly, the medical field.

Chapter two delves into the specific application of vine robots in medicine, particularly in minimally invasive surgery. Its unique design with an outer membrane allows safe navigation through tissues (vessels or neurons), contrasting with other breast cancer diagnosis methods. This feature makes it ideal for addressing challenging anatomical areas and holds promise for minimal invasive surgery applications.

In the third chapter, implemented the modeling of the DC motor with the rack and pinion system. After an examination and understanding of all the forces acting within this dynamic system, these insights were utilized to construct linear graph, normal tree and links. The system's variables were used to formulate state-space equations. State differential equations were developed to describe the system's behavior at each specific time, illustrating the relationships between the system's state variables. Subsequently, the state equations were implemented in MATLAB in order to be integrated using the ode45 function and to simulate the behavior of these state variables according to time, as discussed.

In the fourth chapter, the same approach was followed to construct linear graphs, normal trees, and links for the entire system. This includes the DC motor, rack and pinion dynamics, the active channel linked to the growing element, and the pressurization tank. Detailed analysis was given in the pneumatic system, focusing on Coulomb's friction within the growing element. After the formulation of the state equations, a MATLAB code was implemented again to simulate the behavior of the whole system. The values of the state variables were plotted and the most important output result was that the velocity of the growing element matched that of the active channel simultaneously. This result confirms the accuracy of the modeling and simulation procedures used in this thesis, verifying that the model reflects the system's behavior as described in the MAMMOBOT paper [3]. In the next chapter, a closed-loop control was implemented to regulate this system. The objective was to allow the user to specify the desired velocity of the growing element, and the system would adjust its control signal (voltage source) accordingly to achieve this output. However, due to potentially incorrect parameter values, the simulation did not precisely match all the expected results in the velocities and the current. If the closed-loop application of a proportional controller is successful and yields positive results, the system will become autonomous. The next step will involve simulating vertical motion as well. Eversion growing robots represent a significant advancement in the past decade, with undeniable importance across various fields. Their innovative application in the medical field has the potential to significantly reduce cancer rates by facilitating less invasive procedures. These robots can house catheters internally, minimizing tissue trauma. The everting technology is not limited to cancer detection; it also has the capability to navigate through brain tissue for environmental studies. Another potential application involves extending the capabilities of eversion growing robots to move vertically and in multiple angles. Furthermore, eversion growing robots could be combined with tendon-driven robotic catheters to enhance minimally invasive surgery (MIS).

Bibliography

[1] M. Al-Dubooni, C. Wong, and K. Althoefer. Hybrid continuum-eversion robot: Precise navigation and decontamination in nuclear environments using vine robot. *Arxiv, Cornell University, Computer Science > Robotics*, 19 Apr 2024.

[2] C. Armanini, K. Junge, P. Johnson, C. Whitfield, F. Renda, M. Calisti, and J. Hughes. Soft robotics for farm to fork: applications in agriculture and farming. *IOP Publishing, Bioinspiration and Biomimetics*, 27 February 2024.

[3] P. Berthet-Rayne, S. Sadati, G. Petrou, N. Patel, S. Giannarou, D. R. Leff, and C. Bergeles. Mammobot: A miniature steerable soft growing robot for early breast cancer detection. *IEEE ROBOTICS AND AUTOMATION LETTERS*, 2021.

[4] M. M. Coad, L. H. Blumenschein, S. Cutler, J. A. R. Zepeda, N. D. Naclerio, H. El-Hussieny, U. Mehmood, J.-H. Ryu, E. W. Hawkes, and A. M. Okamura. Vine robots. *IEEE Robotics and Automation Magazine*, 28 November 2019.

[5] P. Flavie, A. Yinoussa, M. Anna, C. Giulio, D. Jeremie, D. Christian, and B.-R. Pierre. 3d kinematics and quasi-statics of a growing robot eversion. *IEEE International Conference on Soft Robotics (RoboSoft)*, 2023.

[6] C. Girerd, A. Alvarez, E. W. Hawkes, and T. K. Morimoto. Material scrunching enables working channels in miniaturized vine-inspired robots. *IEEE TRANSACTIONS ON ROBOTICS, VOL. 40*, 2024.

[7] E. W. Hawkes, L. H. Blumenschein, and J. D. G. A. M. Okamura. A soft robot that navigates its environment through growth. *Science Robotics, Vol 2, Issue 8*, 19 Jul 2017.

[8] M. Li, R. Obregon, J. J. Heit, A. Norbash, E. W. Hawkes, and T. K. Morimoto. Vine catheter for endovascular surgery. *IEEE transactions on medical robotics and bionics*, 2021.

[9] E. Milana. Soft robotics for infrastructure protection. *Frontiers*, 10 November 2022.

[10] M. Motors. Dcx 35 l o35 mm, graphite brushes, ball bearings. https://www.maxongroup.com/maxon/view/product/motor/dcmotor/DCX/DCX35/DCX35L01GBKL604.

[11] W. H. Organization. Breast cancer. https://www.who.int/news-room/fact-sheets/detail/breast-cancer, 2022. [13 March 2024].

[12] W. H. Organization. Global cancer burden growing, amidst mounting need for services. https://www.who.int/news/item/01-02-2024-global-cancer-burden-growing--amidst-mounting-need-for-services, 2022. [1 February 2024].

[13] V. Panagiotis. *Automatic Control System*. University of Thessaly, Department of Computer Science and Biomedical Informatics, 2024.

[14] V. Panagiotis. Lumped parameter dynamic model of an eversion growing robot: Analysis, simulation and experimental validation. *ICRA 2024*, 2024.

[15] V. Panagiotis. *Modeling and Analysis of Dynamic systems*. University of Thessaly, Department of Computer Science and Biomedical Informatics, 2024.

[16] D. Rowell. *Advanced System Dynamics and Control*, chapter Linear Graph Modeling: State Equation Formulation. Massachusetts Institute of Technology, Department of Mechanical Engineering, 2004.

[17] D. Rowell. *Advanced System Dynamics and Control*, chapter Linear Graph Modeling: Two-Port Energy Transducing Elements. Massachusetts Institute of Technology, Department of Mechanical Engineering, 2004.

[18] A. C. Society. Newer and experimental breast imaging tests. https://www.cancer.org/cancer/types/breast-cancer/screening-tests-and-early-detection/experimental-breast-imaging.html, 2022. [January 14, 2022].

[19] Revolutionising neurological disorder treatment with robotics. https://softreach.eu/, 2023.

[20] I. The MathWorks. ode45. https://www.mathworks.com/help/matlab/ref/ode45.html.

[21] I. The MathWorks. Translational friction. https://www.mathworks.com/help/simscape/ref/translationalfriction.html.

[22] Vine robots. https://www.vinerobots.org/.

[23] M. L. Yongde Zhang. A review of recent advancements in soft and flexible robots for medical applications. *The International Journal of Medical Robotics and Computer Assisted Surgery*, 19 February 2020.